iScience

CellPress

Article

Loss of Asb2 Impairs Cardiomyocyte Differentiation and Leads to Congenital Double Outlet Right Ventricle

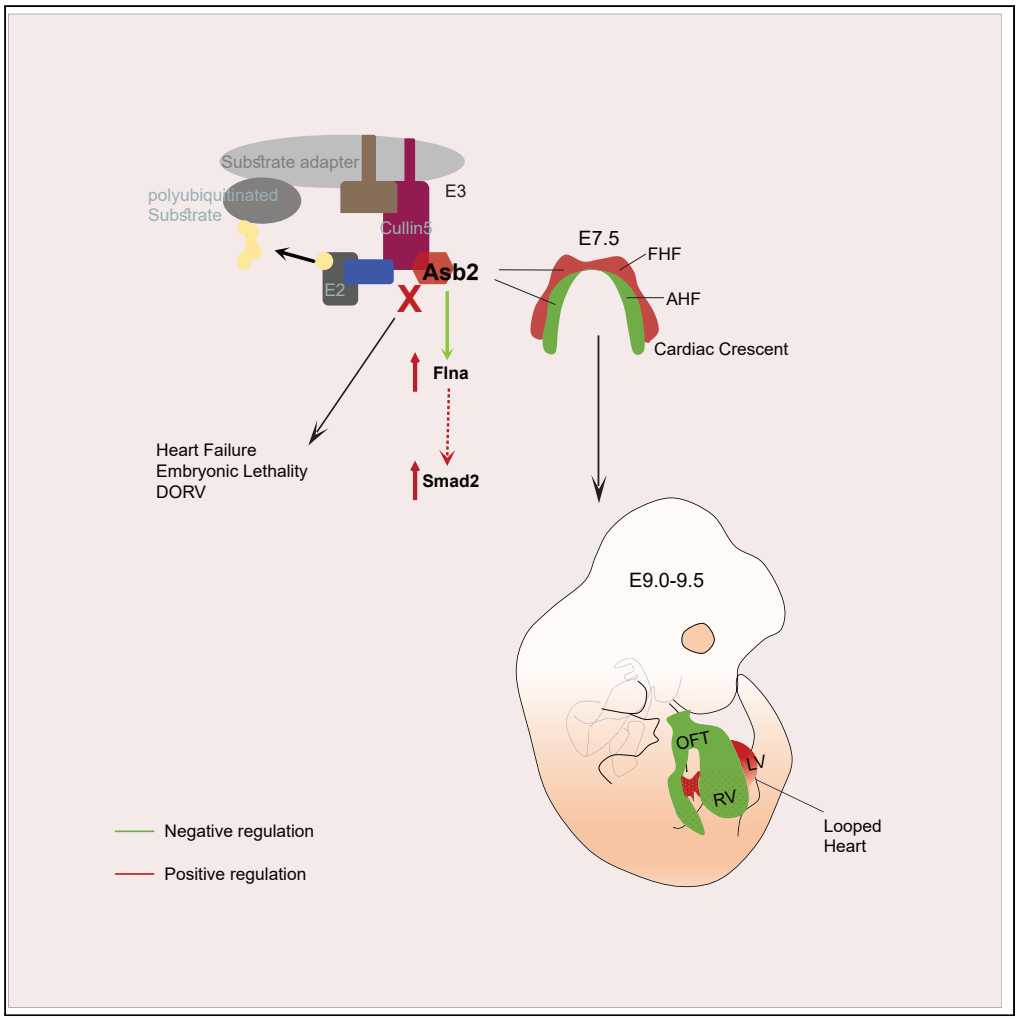

Abir Yamak, Dongjian Hu, Nikhil Mittal, ..., Christel Moog-Lutz, Patrick T. Ellinor, Ibrahim J. Domian

fyamak@mgh.harvard.edu (A.Y.)
idomian@mgh.harvard.edu (I.J.D.)

HIGHLIGHTS

Flna removal partially rescues embryonic lethality of Asb2-heart-specific knockout

AHF-Asb2 knockouts harboring one Flna allele have double outlet right ventricle

Asb2-Flna regulate TGFβ-Smad2 signaling in the heart

Conserved role of Asb2 in heart morphogenesis between mice and humans

DATA AND CODE AVAILABILITY

GSE145495

Yamak et al., iScience *23*, 100959
March 27, 2020
https://doi.org/10.1016/j.isci.2020.100959

iScience

CellPress

Article

Loss of Asb2 Impairs Cardiomyocyte Differentiation and Leads to Congenital Double Outlet Right Ventricle

Abir Yamak,[1,2,3,9,*] Dongjian Hu,[2,4] Nikhil Mittal,[1,2] Jan W. Buikema,[2,5] Sheraz Ditta,[2,6] Pierre G. Lutz,[7] Christel Moog-Lutz,[7] Patrick T. Ellinor,[1,2,3] and Ibrahim J. Domian[1,2,8,*]

SUMMARY

Defining the pathways that control cardiac development facilitates understanding the pathogenesis of congenital heart disease. Herein, we identify enrichment of a Cullin5 Ub ligase key subunit, Asb2, in myocardial progenitors and differentiated cardiomyocytes. Using two conditional murine knockouts, $Nkx^{+/Cre}$.$Asb2^{fl/fl}$ and AHF-Cre.$Asb2^{fl/fl}$, and tissue clarifying technique, we reveal Asb2 requirement for embryonic survival and complete heart looping. Deletion of Asb2 results in upregulation of its target Filamin A (Flna), and concurrent Flna deletion partially rescues embryonic lethality. Conditional AHF-Cre.Asb2 knockouts harboring one Flna allele have double outlet right ventricle (DORV), which is rescued by biallelic Flna excision. Transcriptomic and immunofluorescence analyses identify Tgfβ/Smad as downstream targets of Asb2/Flna. Finally, using CRISPR/Cas9 genome editing, we demonstrate Asb2 requirement for human cardiomyocyte differentiation suggesting a conserved mechanism between mice and humans. Collectively, our study provides deeper mechanistic understanding of the role of the ubiquitin proteasome system in cardiac development and suggests a previously unidentified murine model for DORV.

INTRODUCTION

Congenital heart diseases (CHDs) are prenatal defects that affect the heart's structure and/or function and are the leading cause of infant mortality under 1 year of age. Approximately 1%–2% of human babies are born with cardiac malformations that pose as major risk factors for adult cardiovascular problems (Bruneau, 2008; Nemer, 2008). The heart, the first functional organ in the developing embryo, starts to form early on during development, before the end of gastrulation. The first and second heart fields (FHF and SHF, respectively) as well as the proepicardial organ and the cardiac neural crest are the major contributors to the forming heart (Martinsen and Lohr, 2015). The FHF gives rise primarily to the left ventricle and most of the atria; the SHF contributes to the right ventricle, outflow tract, and parts of the atria (Srivastava, 2006; Yamak and Nemer, 2015). Induction of the cardiac fate and the proper morphogenesis of the vertebrate heart are controlled by a well-characterized and highly conserved combinatorial network of transcription factors and signaling molecules that act together to orchestrate the embryonic development of the four-chambered mammalian heart and the subsequent post-natal maturation. Of important note, the adult heart has minimal intrinsic regenerative capacity (Mercola et al., 2011). As a result, significant stressors on the heart can result in loss of viable or functional myocardial tissue and ultimately heart failure. This renders cardiovascular disease a leading cause of death worldwide and highlights an unmet clinical need for novel approaches for heart regeneration. One major approach is the use of stem cells that can be induced to give rise to the different cell types that constitute the heart. Understanding the cellular processes and signaling pathways that govern *in vivo* heart formation and maturation is necessary for the generation of functional mature cardiac tissue for clinical and preclinical applications (Hu et al., 2018).

Targeted protein degradation by the ubiquitin proteasome system (UPS) is important for the regulation of cellular physiology and is required for normal organ formation (Glickman and Ciechanover, 2002). The UPS consists of three enzymes: Ubiquitin (Ub) activating enzyme, E1, which transfers activated Ub to the Ub conjugating enzyme, E2. This then interacts with the E3 Ub ligase that covalently links the Ub or Ub chain to a lysine residue in the substrate thus targeting it for degradation by the proteasome. The E3 Ub ligase is responsible for substrate specificity (Jung et al., 2009). Recent evidence points to a role of the UPS in heart disease, particularly in myocardial remodeling, familial cardiomyopathies, chronic heart failure, and

[1]Harvard Medical School, Boston, MA 02115, USA

[2]Cardiovascular Research Center, Massachusetts General Hospital, 185 Cambridge Street, CPZN3200, Boston, MA 02114, USA

[3]Cardiovascular Disease Initiative, Broad Institute of MIT and Harvard, Cambridge, MA 02142, USA

[4]Department of Biomedical Engineering, Boston University, Boston, MA 02215, USA

[5]University Medical Center Utrecht, 3584 CX Utrecht, Netherlands

[6]Department of Pharmaceutical Sciences, Utrecht University, 3512 JE Utrecht, Netherlands

[7]Institut de Pharmacologie et de Biologie Structurale, IPBS, Université de Toulouse, CNRS, UPS, Toulouse, France

[8]Harvard Stem Cell Institute, Cambridge, MA 02138, USA

[9]Lead Contact

*Correspondence: fyamak@mgh.harvard.edu (A.Y.), idomian@mgh.harvard.edu (I.J.D.)

https://doi.org/10.1016/j.isci.2020.100959

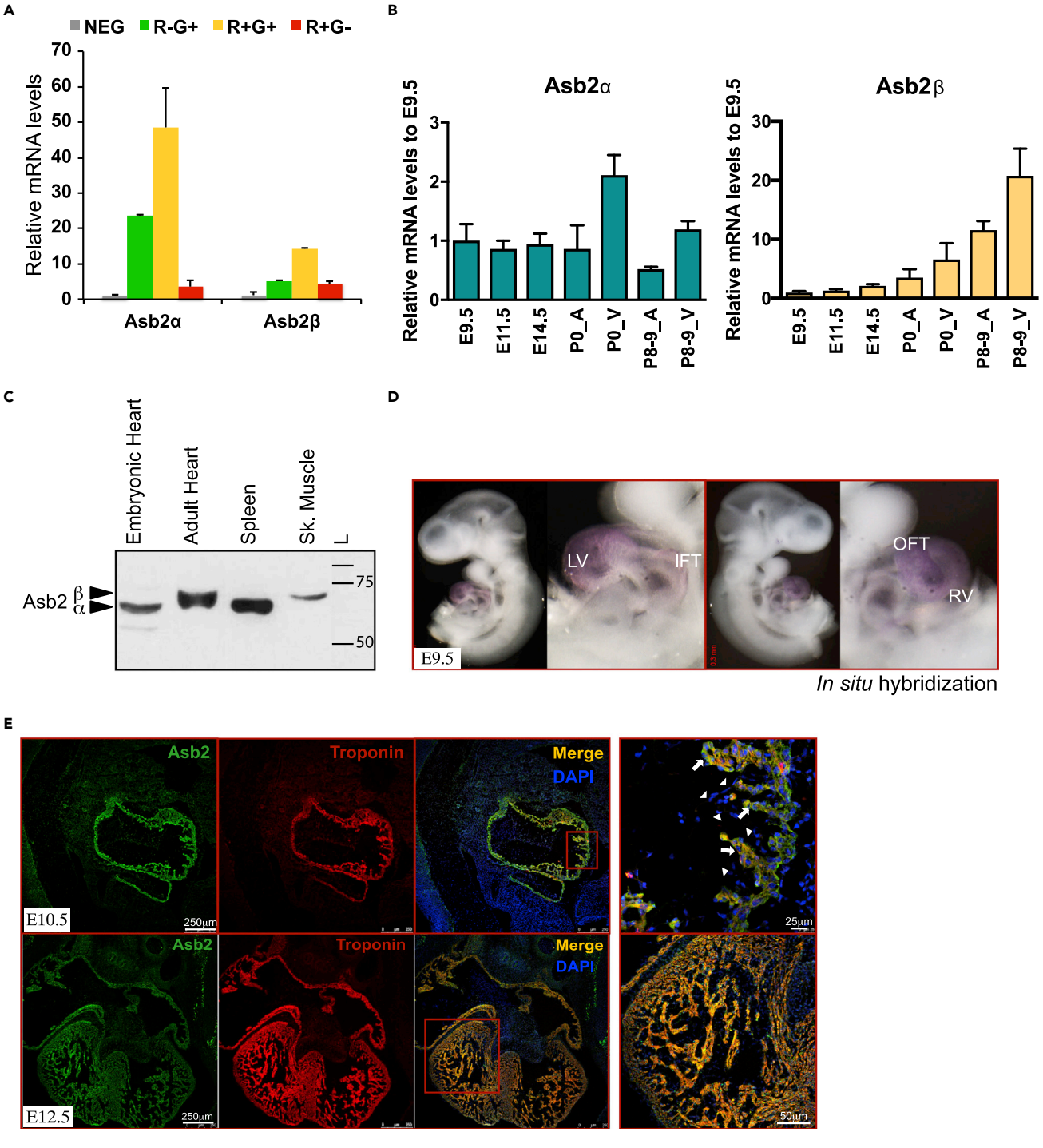

Figure 1. Asb2 Is Expressed in the Developing and Adult Heart and Undergoes Isoform Switching during Differentiation

(A) qPCR analysis of embryonic cardiomyocytes reveals predominant Asb2α expression in the R-G+ and the R+G+ populations. R-G+: Mef2c-.Nkx2-5+; R+G+: Mef2c+.Nkx2-5+; R+G-: Mef2c+.Nkx2-5-; NEG: Mef2c-.Nkx2-5-.

(B) qPCR analysis of Asb2α and Asb2β on RNA from murine hearts of different embryonic stages as well as neonates and postnatal day 8–9. Note that the α isoform is equally expressed at all stages, whereas the β isoform expression increases with development.

(C) Western blot analysis on whole tissue extracts from embryonic and adult heart, spleen, and skeletal muscle using Asb2-specific antibody. Note that Asb2 corresponding band in the embryonic heart co-migrates with that in the spleen where only the α isoform is expressed, whereas that in the adult heart co-migrates with that in the skeletal muscle that is known to express on the β isoform. These data are consistent with the qPCR data in (B).

Figure 1. *Continued*

(D) *In situ* hybridization on E9.5 mouse embryo showing robust Asb2 expression in the LV, RV, and OFT and to a lesser extent the IFT. LV, left ventricle; RV, right ventricle; OFT, outflow tract; IFT, inflow tract.

(E) Immunohistochemistry on E10.5 and E12.5 mouse embryos using Asb2-specific antibody (green) and Troponin T (red). DAPI (blue) marks nuclei. Note Asb2 expression colocalizes with Troponin T in the myocardium (arrows) and no expression is seen in the endocardial cells (arrow heads). Scale bar is equivalent to 250 μm in the first three heart images left to right at E10.5 (top) and E12.5 (bottom), 25 μm in the E10.5 heart image top far right, and 50 μm in the E12.5 heart image bottom far right as indicated in the figure.

ischemia-reperfusion injury (Pagan et al., 2013). Pharmacological inhibition of the proteasome is a new and promising means for cardioprotection (Pagan et al., 2013). Paradoxically, enhancing UPS activity has in some cases also provided protection against heart disease (Bulteau et al., 2001; Li et al., 2011; Powell et al., 2007) highlighting the importance of defining the role of the UPS as a therapeutic target in cardiac disease. In addition to its role as a protein quality control, the UPS has also been shown to regulate the turnover of sarcomere proteins, including the myofibrillar proteins myosin, actin, and troponin. Examples of this include the E3 Ub ligases MuRF1 (muscle-specific RING finger 1, targeting troponin I) and F box protein Fbx122 (targeting α-actinin and filamin C) (Kedar et al., 2004; Spaich et al., 2012). E3 ligases have also been shown to regulate important signaling pathways in the heart, such as the JNK (c-Jun N terminal kinase) (Laine and Ronai, 2005), calcineurin (Fan et al., 2008), and the VEGF (vascular endothelial growth factor) signaling pathways (Murdaca et al., 2004). This important role of the UPS in the heart and its potential for a therapeutic target in cardiac disease brings about a need to understand its specific function in heart development and disease. Using our previously described transgenic reporter system (Domian et al., 2009), we identified Asb2 (ankyrin repeat-containing protein with a suppressor of cytokine signaling box [SOCS box] 2) as being enriched in FHF and SHF cardiac progenitors. Asb2, which encodes specificity subunit of Cullin 5 RING E3 Ub ligase, exists in two isoforms: Asb2α and Asb2β in mouse, corresponding to variants 2 and 1 in humans, respectively (Bello et al., 2009). It has previously been shown to regulate differentiation of myeloid leukemia cells and skeletal myogenesis through proteasomal degradation of filamin proteins (Bello et al., 2009; Guibal et al., 2002; Heuzé et al., 2008). Filamins (Flna, Flnb, and Flnc in mice) are actin-binding proteins important for the stabilization of the actin-cytoskeleton (van der Flier and Sonnenberg, 2001). Flnc is the only isoform expressed in the heart muscle where it is required for normal contractility (Fujita et al., 2012). Flna expression in the heart is restricted to endocardial and mesenchymal cells of the cardiac cushions during development and to valve leaflets in the adult heart (Norris et al., 2010). FLNA and FLNC mutations have been linked to cardiac defects in humans (de Wit et al., 2011, 2009; Kyndt et al., 2007; Valdés-Mas et al., 2014). In zebrafish, an additional Asb2 target TCF3 was very recently identified where TCF3 was negatively regulated by Asb2 during cardiogenesis (Fukuda et al., 2017). Asb2 downregulation was also shown to be a mediator of follistatin-induced muscle hypertrophy and SMAD2/3 regulation of skeletal muscle mass in young adults in mice. The repression of Asb2 was, however, ameliorated in aging mice, some of which also displayed increasing Asb2 baseline levels (Davey et al., 2016). Asb2 overexpression was also shown to drive skeletal muscle atrophy in mice (Davey et al., 2016). A recent study also showed that Asb2 knockout is embryonic lethal and that Asb2α targets Flna for proteasomal degradation during early cardiomyocyte differentiation (Métais et al., 2018). The embryonic lethality of Asb2 mutants was shown to be primarily due to heart defects (Métais et al., 2018).

Herein, we show that Asb2 knockout in the FHF and SHF are both embryonic lethal by E10.5 and E12.5, respectively. Using tissue clearing combined with immunofluorescence technique, we show that Asb2 mutant hearts have incomplete looping. Moreover, Asb2 regulates cardiac morphogenesis partly through Flna turnover, and we hereby propose a model where Asb2-Flna controls TGFβ-SMAD signaling to drive early cardiac formation. Additionally, Asb2 lethality in the anterior heart field (AHF) is partially rescued by Flna removal from these hearts. We also show that Asb2 ablation in the AHF leads to double outlet right ventricle (DORV), which is corrected upon further deletion of Flna from these hearts. Finally, we reveal that Asb2 role in cardiomyocyte differentiation is conserved in human cardiomyocytes as well. Collectively, our results shed light on the UPS regulation of heart development and its role as a cardio-therapeutic target and provide evidence for the first time for the role of the UPS in the rare congenital heart defect, DORV.

RESULTS

Asb2 Is Highly Enriched in the Embryonic Heart

We have previously characterized a transgenic reporter system for the isolation of three distinct mouse cardiac progenitor cells from developing embryos: FHF population, marked by Nkx2.5+.Mef2c- expression, and two SHF population subsets: Nkx2.5-.Mef2c+ and Nkx2.5+.Mef2c+ (Domian et al., 2009). Genome-wide

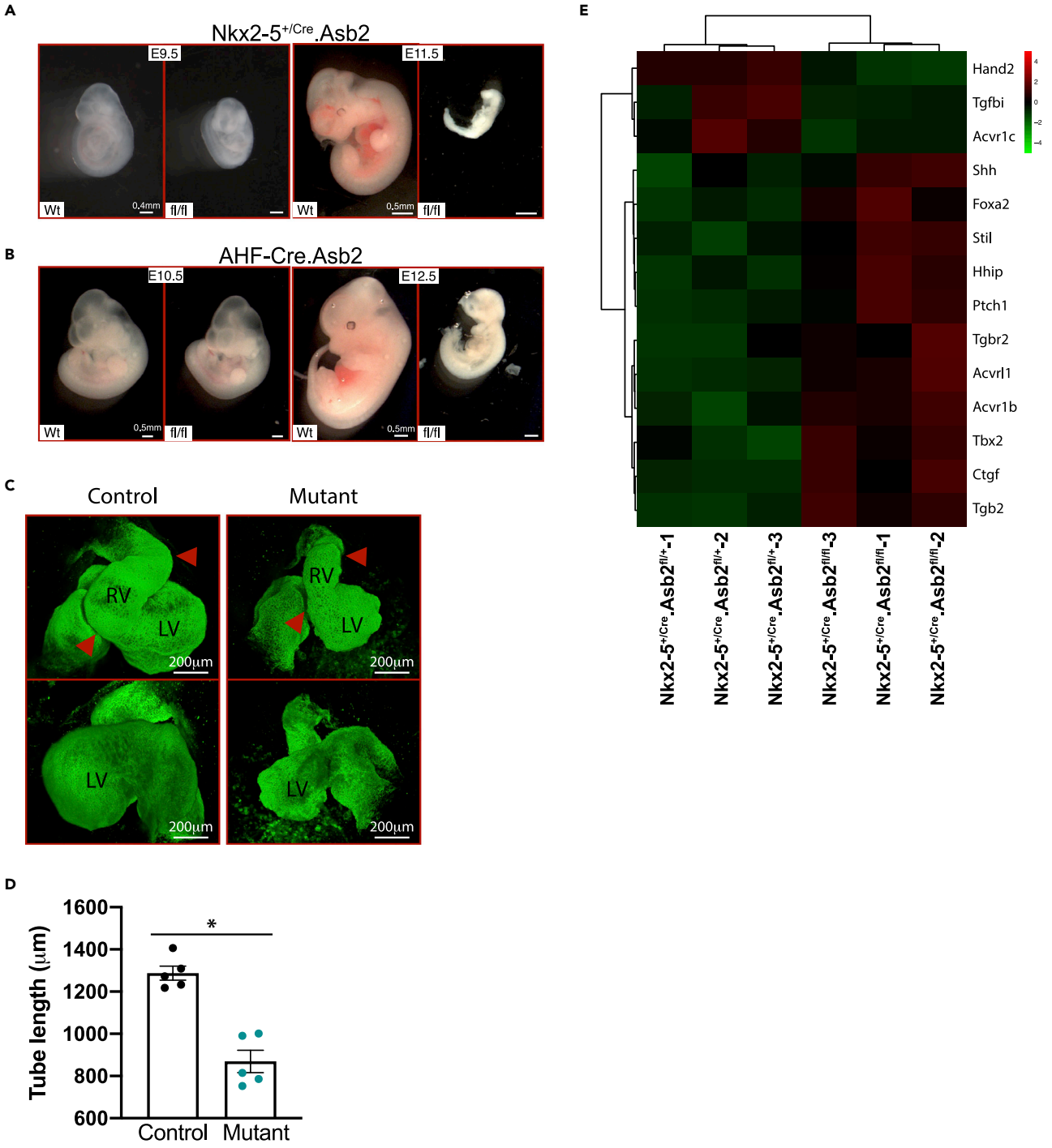

Figure 2. Asb2 Is Essential for Early Cardiac Development

(A) Nkx2-5$^{+/Cre}$.Asb2 E9.5 and E11.5 knockout (KO) embryos (fl/fl) versus wild-type littermates (Wt). Note the resorbing KO embryo at E11.5. Scale bar is equivalent to 0.4 mm for E9.5 and 0.5 mm for E11.5 as indicated.

(B) AHF-Cre.Asb2 E10.5 and E12.5 knockout (KO) embryos (fl/fl) versus wild-type littermates (Wt). Note the resorbing KO embryo at E12.5. Scale bar is equivalent to 0.5 mm for E10.5 and E12.5 as indicated in the figure.

(C) 3D reconstruction of CUBIC-cleared, Troponin-T-stained E9.5 whole control and Asb2 mutant embryos showing both ventral and dorsal views. Note the bulging in the right ventricle of the control heart that is lacking in the mutant (indicated by the red arrow heads). Scale bar is equivalent to 200 μm as indicated.

Figure 2. *Continued*

(D) Measurement of the heart tube of control and Asb2 mutant hearts. Note the statistically significant shorter heart tubes of the mutants. N = 5 per group. Data are represented as mean ± SEM. * = $p < 0.005$. Unpaired t test was used using GraphPad Prism; $p < 0.05$ is considered statistically significant. (E) Heatmap analysis of a subset of cardiac looping differentially expressed genes in RNA-seq data from control (Nkx2-5$^{+/Cre}$.Asb2$^{fl/+}$) versus Nkx2-5$^{+/Cre}$.Asb2 knockout E9.5 murine hearts. N = 3 in each group (each sample is in itself a combination of three to four hearts to account for heterogeneity among different litters).

transcriptional profiling and real-time PCR (qPCR) reveal Asb2 transcripts enrichment in the three populations (Figure 1A) (Domian et al., 2009). To investigate the temporal expression of Asb2 in the developing heart, we performed qPCR analysis on RNA from mouse hearts at different stages of embryonic development. Our data show that Asb2α is expressed similarly throughout heart development, whereas Asb2β expression increases with development (Figure 1B). This is further confirmed by western blot analysis, which shows that the Asb2 band in the embryonic heart co-migrates with that in the spleen (which expresses Asb2α [Spinner et al., 2015]), whereas the Asb2 band in the adult heart co-migrates with that in the skeletal muscle (known to express Asb2β [Bello et al., 2009]) (Figure 1C). To further investigate *in vivo* spatial cardiac expression of Abs2, we performed *in situ* hybridization on E9.5 embryos. Our data reveal robust expression of Asb2 transcripts predominantly in the left (LV) and right ventricles (RV) and to a lower extent in inflow (IFT) and outflow tracts (OFT) (Figure 1D). Furthermore, immunostaining of E10.5 and E11.5 (Figure 1E, upper and lower panels, respectively) embryonic sections using Asb2-specific antibody shows that, in the heart, Asb2 expression (green) is restricted to the myocardium overlapping with cardiac Troponin T (red). White arrows in the zoomed merged image at E10.5 (right panel) indicate overlap of Asb2 and Troponin T in the myocardial layer, but no expression is seen in the endocardial layer indicated by arrow heads.

Asb2 Is Required for Early Cardiac Formation

To investigate the role of Asb2 during cardiac development, we generated two conditional knockout lines (KO): Nkx2-5$^{+/Cre}$ (a mouse line with the Cre recombinase knocked into the Nkx2-5 locus) and AHF-Cre (a mouse line with a transgene placing Cre under the transcriptional control of the AHF enhancer of the Mef2c gene). These mouse lines allow for the targeted removal of (Lombardi et al., 2009) Asb2 from the whole heart and the SHF, respectively (Lombardi et al., 2009). The floxed alleles are in common region and inactivate both Asb2 isoforms. Both conditional KOs have pericardial edema and are embryonic lethal: Nkx2-5$^{+/Cre}$.Asb2$^{fl/fl}$ mice die at E10.5–11 and AHF-Cre.Asb2$^{fl/fl}$ die at E11.5–12 (Figures 2A and 2B, respectively). AHF-Cre.Asb2$^{fl/fl}$ mice analyzed at E10.5 also have shorter OFT compared with their control littermates (Figure S1D). For Nkx2-5$^{+/Cre}$.Asb2$^{fl/fl}$, mice were analyzed at E8.5 (3 litters), E9.5 (23 litters), E10.5 (3 litters), and E11.5 (2 litters); for AHF-Cre.Asb2$^{fl/fl}$, mice were analyzed at E9.5 (3 litters), E10.5 (4 litters), and E12.5 (2 litters). Each litter consists of 8–11 embryos in total. All embryos were genotyped. Figure S1A shows the reduced level of Asb2 in the heterozygotes (Nkx2-5$^{+/Cre}$.Asb2$^{fl/+}$) and the complete loss of Asb2 in the knockouts (Nkx2-5$^{+/Cre}$.Asb2$^{fl/fl}$).

In order to perform a phenotypic analysis of the Nkx2-5$^{+/Cre}$-Asb2$^{fl/fl}$ mutant embryos, we used state-of-the-art tissue clearing technique CUBIC combined with immunostaining. CUBIC can effectively clear mice embryos and embryonic hearts while preserving immunolabels (Kolesová et al., 2016; Tainaka et al., 2014). Nkx2-5$^{+/Cre}$-Asb2$^{fl/fl}$ and control littermates e9.5 mice embryos were cleared with CUBIC and stained for Troponin T to mark cardiomyocytes as well as DAPI for nuclei. Confocal microscopy with optical sectioning followed by 3D-reconstruction allowed the precise visualization of the developing hearts without disruption of underlying anatomy. During cardiac morphogenesis, the straight heart tube undergoes sequential looping steps to get to the fully looped heart. The fully looped heart acquires a helical shape in mice that is also referred to as the mature S-loop in chicks (Le Garrec et al., 2017; Männer, 2009). In Le Garrec et al. paper, they used computer modeling to simulate the biological process of mouse cardiac looping, incorporating in their model the left-right asymmetry and mechanical constraints seen in the looping heart. Their findings suggest that the lack of any of these parameters would lead to a C-shaped heart loop rather than the helical structure. In the chick, the heart is first transformed into a C-shaped heart, a process known as dextral looping. The C-loop is then converted into an immature S-loop that then transforms into a mature S-looped heart where the ventricular segments are curved outward to generate the left and right chambers (Männer, 2009). As shown in Figure 2C, the mutant embryos do not form the full helical structure seen in the control littermates. Instead, they have partially looped hearts that resemble the C-shaped hearts in the chick (Männer, 2009). Moreover, measurement of the heart tube length in mutant versus control hearts reveals statistically significant shorter tubes in the mutant hearts (Figure 2D). Video S1 is a z stack of stained control and mutant e9.5 embryos showing the incomplete looping in the mutant embryo. Figure S1C represents four images from the z stack at different depth in the embryo. Four to five

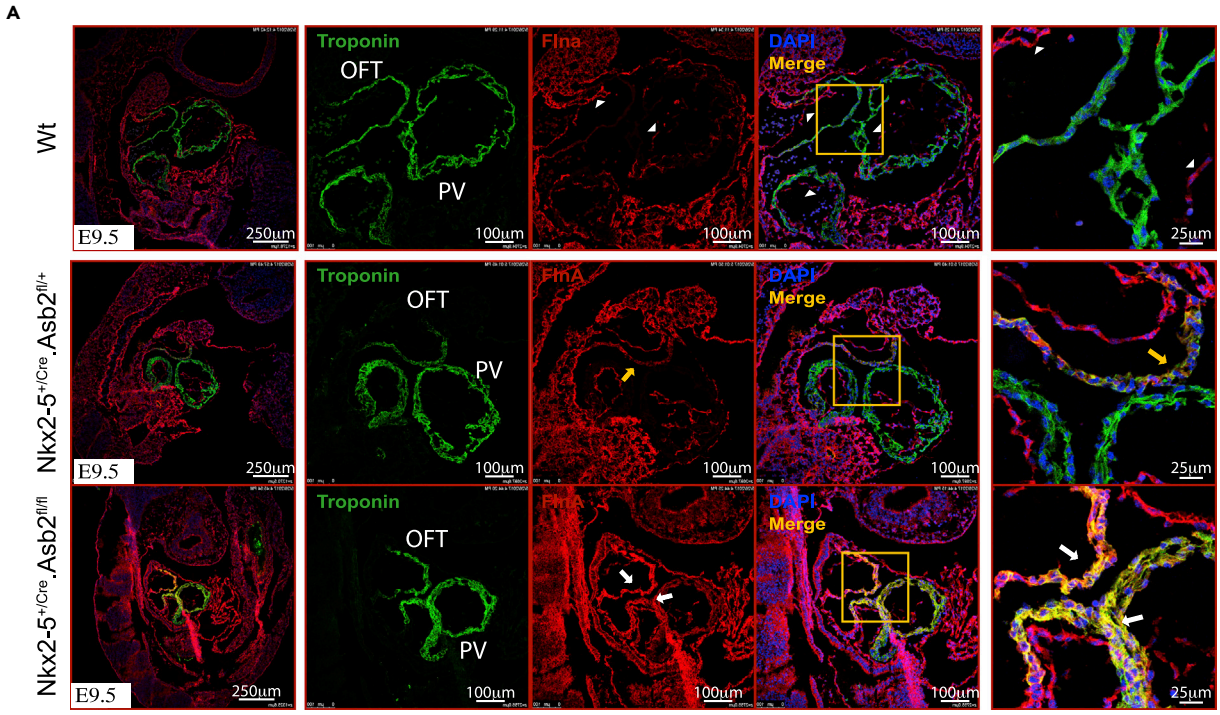
A
Wt
Nkx2-5+/Cre.Asb2fl/+
Nkx2-5+/Cre.Asb2fl/fl
Troponin
OFT
PV
Flna
DAPI
Merge
E9.5
250μm
100μm
25μm

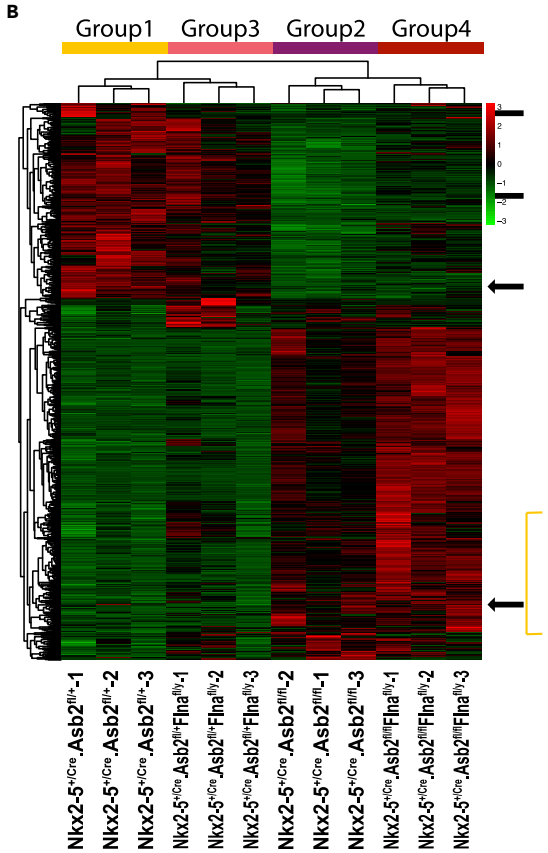
B
Group1
Group3
Group2
Group4
Nkx2-5+/Cre.Asb2fl/+-1
Nkx2-5+/Cre.Asb2fl/+-2
Nkx2-5+/Cre.Asb2fl/+-3
Nkx2-5+/Cre.Asb2fl/+Flnafl/fl-1
Nkx2-5+/Cre.Asb2fl/+Flnafl/fl-2
Nkx2-5+/Cre.Asb2fl/+Flnafl/fl-3
Nkx2-5+/Cre.Asb2fl/fl-2
Nkx2-5+/Cre.Asb2fl/fl-1
Nkx2-5+/Cre.Asb2fl/fl-3
Nkx2-5+/Cre.Asb2fl/flFlnafl/fl-1
Nkx2-5+/Cre.Asb2fl/flFlnafl/fl-2
Nkx2-5+/Cre.Asb2fl/flFlnafl/fl-3

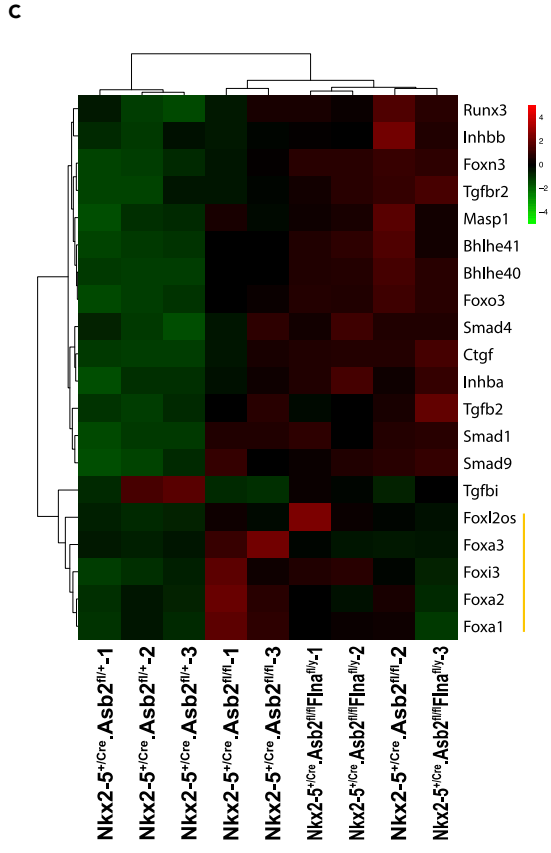
C
Runx3
Inhbb
Foxn3
Tgfbr2
Masp1
Bhlhe41
Bhlhe40
Foxo3
Smad4
Ctgf
Inhba
Tgfb2
Smad1
Smad9
Tgfbi
Foxl2os
Foxa3
Foxi3
Foxa2
Foxa1
Nkx2-5+/Cre.Asb2fl/+-1
Nkx2-5+/Cre.Asb2fl/+-2
Nkx2-5+/Cre.Asb2fl/+-3
Nkx2-5+/Cre.Asb2fl/fl-1
Nkx2-5+/Cre.Asb2fl/fl-3
Nkx2-5+/Cre.Asb2fl/flFlnafl/fl-1
Nkx2-5+/Cre.Asb2fl/flFlnafl/fl-2
Nkx2-5+/Cre.Asb2fl/fl-2
Nkx2-5+/Cre.Asb2fl/flFlnafl/fl-3

Figure 3. Asb2 Targets Flna for Proteasomal Degradation in the Developing Heart and Asb2-Mutant Hearts Have an Altered Gene Expression Profile

(A) Immunohistochemistry on E9.5 Abs2 heterozygote (Nkx2-5$^{+/Cre}$.Asb2$^{fl/+}$, middle pane) and mutant hearts (Nkx2-5$^{+/Cre}$.Asb2$^{fl/fl}$, lower panel) as well as Wt controls (top panel) using Flna (red) and Troponin-T (green)-specific antibodies. Note that FlnA expression is restricted to the endocardial layer (white arrow heads) in the Wt heart, whereas it is abnormally expressed in the myocardial layer in the Asb2-mutant hearts co-localizing with Troponin-T expression there (white arrows). Moreover, some cardiomyocytes in the outflow tract of the Asb2-heterozygous hearts also express Flna (yellow arrows) suggesting a dose-dependent regulation. Scale bar is equivalent to 250 μm in the first column (left), 100 μm in the second, third, and fourth columns, and 25 μm in the fifth (far right) column as indicated in the figure.

(B) Heatmap analysis of RNA-seq data from control (Group1: Nkx2-5$^{+/Cre}$.Asb2$^{fl/+}$), Asb2 mutant (Group2: Nkx2-5$^{+/Cre}$.Asb2$^{fl/fl}$), Flna mutant (Group3: Nkx2-5$^{+/Cre}$.Flna$^{fl/y}$), and Asb2-Flna double mutant (Group4: Nkx2-5$^{+/Cre}$.Asb2$^{fl/fl}$.Flna$^{fl/y}$) E9.5 murine hearts. Note the high level of differentially expressed genes in the Asb2-mutant and Asb2-Flna double mutant versus the control groups. A small subset of genes (indicated by arrows) that are perturbed in the Asb2-mutant hearts are restored to normal in the Asb2-Flna double mutants. N = 3 in each group (each sample is in itself a combination of three to four hearts to account for heterogeneity among different litters).

(C) Heatmap analysis of a subset of genes from the RNA-seq data in (B) that are part of the Tgfβ/Smad signaling pathway. Note that the Foxa genes expression levels (indicated with a yellow line) that are downstream of the Tgfβ/Smad are restored to normal in the Asb2-Flna double mutants versus the Asb2-mutant hearts.

embryos were analyzed for each condition. The efficiency of the CUBIC/immunostaining technique on e9.5 mouse embryo is evidenced by the clearly visible striations of the cardiac muscle fibers (Figure S1B).

In order to identify Asb2 downstream targets in the heart, RNA sequencing (RNA-seq) analysis was performed on Nkx2-5$^{+/Cre}$.Asb2$^{fl/fl}$ and control littermates (Figure 3B) (Figure S2C shows reduced levels of Asb2 transcripts in the Nkx2-5$^{+/Cre}$.Asb2$^{fl/fl}$ knockout compared with the Nkx2-5$^{+/Cre}$.Asb2$^{fl/+}$ heterozygote control). The gene expression profile was greatly altered in the Asb2 mutant hearts compared with their control littermates (Group 2 versus Group 1) (Figure 3B). Of note, a number of genes that are mis-expressed in the Asb2 cardiac mutant hearts have been previously linked to abnormal cardiac looping in mice (Figure 2E) (Azhar et al., 2003; Bardot et al., 2017; Chen et al., 1997; Le Garrec et al., 2017; Mine et al., 2008; Ribeiro et al., 2007; Vincentz et al., 2011). Ingenuity Pathway Analysis also shows that "cardiovascular system development and function" as well as "cardiovascular disease" are among the top pathways altered in the Asb2 mutant hearts (Table S1, yellow highlights). Table S2 is an upstream analysis with the ones with a positive activation *Z* score > 1.5 highlighted in yellow. This list shows the pathways whose downstream targets are altered (upregulated or downregulated) in our knockouts versus controls. Targets with a positive *Z* score suggest upregulation pathways in the Asb2 mutant hearts.

Asb2 Controls Cardiac Morphogenesis Partly through Regulating Filamin A

Since Asb2 targets filamin proteins for degradation (Métais et al., 2018) and Flna perturbations lead to cardiac defects and embryonic lethality (Feng et al., 2006), we investigated cardiac Flna expression in the Nkx2-5$^{+/Cre}$.Asb2$^{fl/fl}$. Flna expression in the control heart (Figure 3A, top panel) is restricted to endocardial and pericardial layers (red staining, white arrow heads). In the knockout embryos (Figure 3A, third panel), Flna's expression domain is abnormally expanded to include the myocardial layer (white arrows), co-localizing with Troponin T expression (green for Troponin and yellow for the co-localization). Moreover, in Nkx2-5$^{+/Cre}$.Asb2$^{fl/+}$ heterozygous hearts (Figure 3A, second panel), Flna is abnormally expressed in some cardiomyocytes of the OFT myocardium (yellow arrows) suggesting that Asb2 regulation of Flna turnover is dose dependent. We then hypothesized that, if Asb2 cardiac mutant phenotype is due to overexpression of Flna, then concurrently deleting Flna along with Asb2 should suppress the Asb2 phenotype. (Please note that Flna is an x-linked gene so a knockout is denoted by fl/fl for female or fl/y for male, whereas a heterozygous is denoted by fl/x or fl/+.) To examine this hypothesis, we developed Nkx2-5$^{+/Cre}$.Asb2$^{fl/fl}$.Flna$^{fl/y}$ double mutants. Removal of Flna from the hearts of Nkx2-5$^{+/Cre}$.Asb2$^{fl/fl}$ did not rescue lethality (Figure S2A). Approximately 16 litters were analyzed at E9.5 and 3 litters at E10.5. As expected, Nkx2-5$^{+/Cre}$.Asb2$^{fl/fl}$.Flna$^{fl/fl}$ double knockouts no longer harbor ectopic Flna expression in the myocardium (Figure S2B) as was previously seen with the Nkx2-5$^{+/Cre}$.Asb2$^{fl/fl}$ single knockouts (Figure 3A). Instead, the double knockouts have normal endocardial expression of Flna similar to their control littermates (Figure S2B). RNA-seq analysis on e9.5 hearts from these mice show that their gene expression profile is closely related to the Nkx2-5$^{+/Cre}$.Asb2$^{fl/fl}$ group (Group 2 versus Group 4) (Figure S2C shows reduced levels of Asb2 transcripts in the Nkx2-5$^{+/Cre}$.Asb2$^{fl/fl}$.Flna$^{fl/y}$ double knockout compared with the Nkx2-5$^{+/Cre}$.Asb2$^{fl/+}$ heterozygote control). However, some genes whose expression was altered in the Nkx2-5$^{+/Cre}$.Asb2$^{fl/fl}$ group are restored to normal in the Nkx2-5$^{+/Cre}$.Asb2$^{fl/fl}$.Flna$^{fl/y}$ hearts (indicated by arrows and shown in Table S3). These results suggest that Flna concurrent deletion can restore the normal expression level of a subset of genes in the Asb2 mutant hearts. Among these genes are the

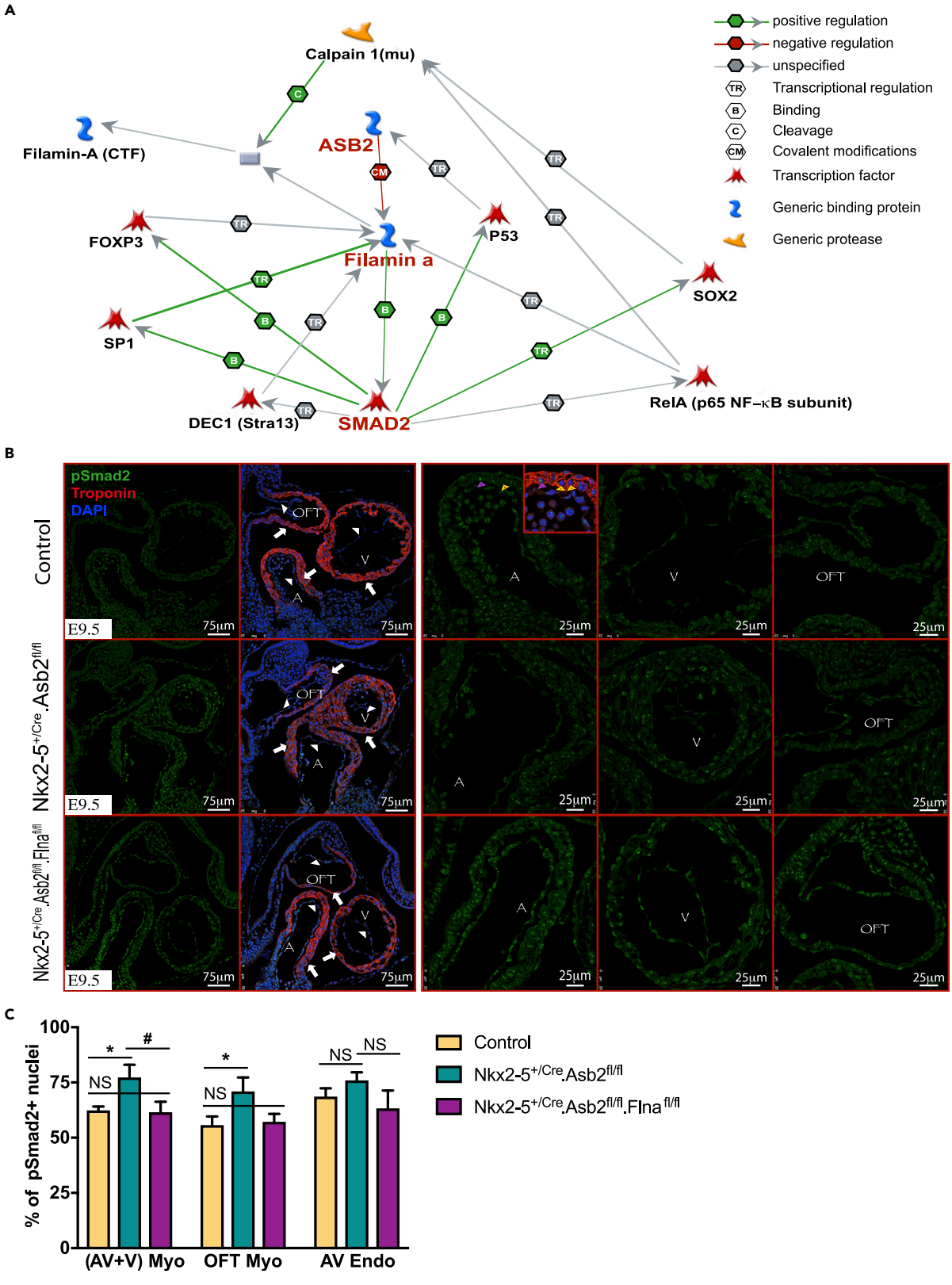
A
Calpain 1(mu)
Filamin-A (CTF)
ASB2
FOXP3
P53
Filamin a
SOX2
SP1
DEC1 (Stra13)
SMAD2
RelA (p65 NF–κB subunit)
positive regulation
negative regulation
unspecified
Transcriptional regulation
Binding
Cleavage
Covalent modifications
Transcription factor
Generic binding protein
Generic protease
B
pSmad2
Troponin
DAPI
Control
Nkx2-5+/Cre.Asb2fl/fl
Nkx2-5+/Cre.Asb2fl/fl.Flnafl/fl
E9.5
75μm
25μm
OFT
V
A
C
% of pSmad2+ nuclei
100
75
50
25
0
NS
*
#
(AV+V) Myo
OFT Myo
AV Endo
Control
Nkx2-5+/Cre.Asb2fl/fl
Nkx2-5+/Cre.Asb2fl/fl.Flnafl/fl

Figure 4. Tgfβ/Smad Signaling Activity Is Downstream Asb2-Flna in the Developing Heart

(A) Schematic representation of Asb2-Flna-Smad2 interaction network using MetaCore Clarivate Analytics software. Note that Asb2 ubiquitinates and negatively regulates Flna, whereas Flna binds directly to and positively regulates Smad2.

(B) Immunohistochemistry on Nkx2-5$^{+/Cre}$.Asb2 mutant (middle panel) and Nkx2-5$^{+/Cre}$.Asb2-Flna double mutant (last panel) murine hearts as well as wild-type controls (top panel) using pSmad2-specific antibody (green) and Troponin T (red). Note the nuclear localization of pSmad2 as a sign of Tgfβ/Smad2 cycle activation. Examples of positive (purple arrowhead) and negative (yellow arrowheads) nuclei are indicated in the Wt sample (red box). DAPI marks all nuclei (AV, atrioventricular canal; V, primitive ventricle; OFT, outflow tract; Myo, myocytes; Endo, endocardial cells). Myocardial cells are marked by white arrows; endocardial cells are marked by white arrowheads. Scale bar is equivalent to 75 μm in the first two columns from the left and 25 μm in the third, fourth, and fifth columns as indicated in the figure.

(C) Quantification of the immunostaining in (B) of percentage of pSmad2-positive nuclei in cardiomyocytes ((AV+V) Myo and OFT Myo) as well as endocardial cells (AV endo). Note the increased level of pSmad2-positive nuclei in Asb2-mutant myocytes that are restored to normal in the Asb2-FlnA double mutants. This regulation is not seen in the endocardial cells that do not express Asb2 (Figure 1E). n = 7 for Wt; n = 4 for Nkx2-5$^{+/Cre}$.Asb2$^{fl/fl}$; n = 3 for Nkx2-5$^{+/Cre}$.Asb2$^{fl/fl}$.Flna$^{fl/fl}$. Data are represented as mean ± SEM. * = $p < 0.05$ Control versus Nkx2-5$^{+/Cre}$.Asb2$^{fl/fl}$; # = $p < 0.05$ Nkx2-5$^{+/Cre}$.Asb2$^{fl/fl}$ versus Nkx2-5$^{+/Cre}$.Asb2$^{fl/fl}$.Flna$^{fl/fl}$; NS = not significant. Two-way ANOVA was used for analysis using GraphPad Prism. $p < 0.05$ is considered statistically significant.

Foxa genes, which are downstream of the Tgfβ/Smad signaling (Figure 3C, yellow line) (Tang et al., 2011). Other genes in the Tgfβ/Smad pathway are also altered in both Asb2-mutant and Asb2.Flna double mutant hearts (Figure 3C). Figure S2D is a qPCR analysis confirming some of these altered genes. Tgfβr1 and InhA (which encodes a member of the Tgfβ superfamily) are also among the positively regulated targets in the upstream analysis of the RNA-seq data of Asb2-mutant hearts versus control (Table S2). Both genes are no longer positively regulated in the upstream analysis of the list of genes corrected in the Asb2-Flna double mutant hearts (Table S3, yellow highlights). These data prompted further analysis of the Asb2/Flna regulation of TGFβ/Smad signaling in the heart of these mice.

Asb2 Regulates TGFβ/Smad Signaling through Regulating Filamin A Protein

TGFβ signaling is initiated upon ligand-stimulated activation of serine/threonine receptor kinases that in turn lead to phosphorylation and activation of Smad proteins. Activated Smads interact with common signaling transducer Smad4, translocate to the nucleus, and activate downstream targets (Shi and Massagué, 2003). Flna directly associates with Smad2 and Smad2 phosphorylation, and TGFβ/Smad2 signaling is impaired in Fln-null human melanoma cells (Sasaki et al., 2001; Zhou et al., 2011). Moreover, FLNA mutations were linked to x-linked myxomatous valvular dystrophy, a multivalve degeneration disorder, and disrupted TGFβ/Smad2/3 signaling was implicated in the disease pathogenesis (Geirsson et al., 2012; Norris et al., 2010). Using the "Build Network" module in MetaCore Clarivate Analytics software, we investigated the Asb2-Flna-Smad2 interaction. As shown in Figure 4A, Asb2 negatively regulates Flna through ubiquitination and Flna positively regulates Smad2 through direct binding. Asb2, Flna, and Smad2 are shown in red for visualization. In order to investigate further Asb2/Flna regulation of TGFβ/Smad2 signaling in cardiac development, we immunostained E9.5 Asb2-mutant hearts with antisera directed against pSmad2 (Figure 4B) and then quantified the pSmad2-positive nuclei. Figure 4C shows significant increase in the percentage of pSmad2-positive nuclei in the Nkx2-5$^{+/Cre}$.Asb2$^{fl/fl}$ myocytes (previously shown to have overexpression of Flna [Figure 3A]) compared with their littermate controls. This increase was not seen in the endocardial cells where Flna expression is normal (Figure 3A). Interestingly, pSmad2 levels were restored to normal in the Nkx2-5$^{+/Cre}$.Asb2$^{fl/fl}$.Flna$^{fl/fl}$ (double mutant) myocytes further confirming that Asb2 regulates pSmad2 in the heart through the regulated turnover of Flna.

Flna Removal from AHF-Cre.Asb2 Mutant Hearts Partially Rescues Embryonic Lethality

To examine Flna expression in the AHF-Cre.Asb2$^{fl/fl}$ hearts (where Asb2 is knocked out in the RV and OFT only), Flna immunostaining was performed. As shown in Figure 5A, Flna expression (red) is restricted to the endocardial and epicardial layers in the control hearts (top panel, white arrow heads), whereas it is aberrantly expressed in the myocardial layer of the OFT and RV only (red staining lower panel, white arrows), co-localizing with TroponinT expression (yellow staining lower panel) there. Flna expression was normal in the myocardial layer of the primitive left ventricle (PV) that harbors normal Asb2 expression and acts as an internal control in these mice. We then sought to examine the effect of further knocking out Flna from the AHF-Cre.Asb2-mutant hearts. To do this, we crossed Asb2$^{fl/fl}$.Flna$^{fl/fl}$ with AHF-Cre.Asb2$^{fl/+}$ mice. Our results show that AHF-Cre.Asb2$^{fl/fl}$.Flna$^{fl/y}$ are born with the expected Mendelian ratios (Figure 5B); however, newborn pups die between P0.5 and P1.5. These results show that Flna deletion partially rescues Asb2 lethality. The AHF-Cre.Asb2$^{fl/fl}$.Flna$^{fl/+}$ also survive to birth albeit at a lower percentage from what is expected by Mendelian ratios; these mice also die right after birth at P0.5.

A

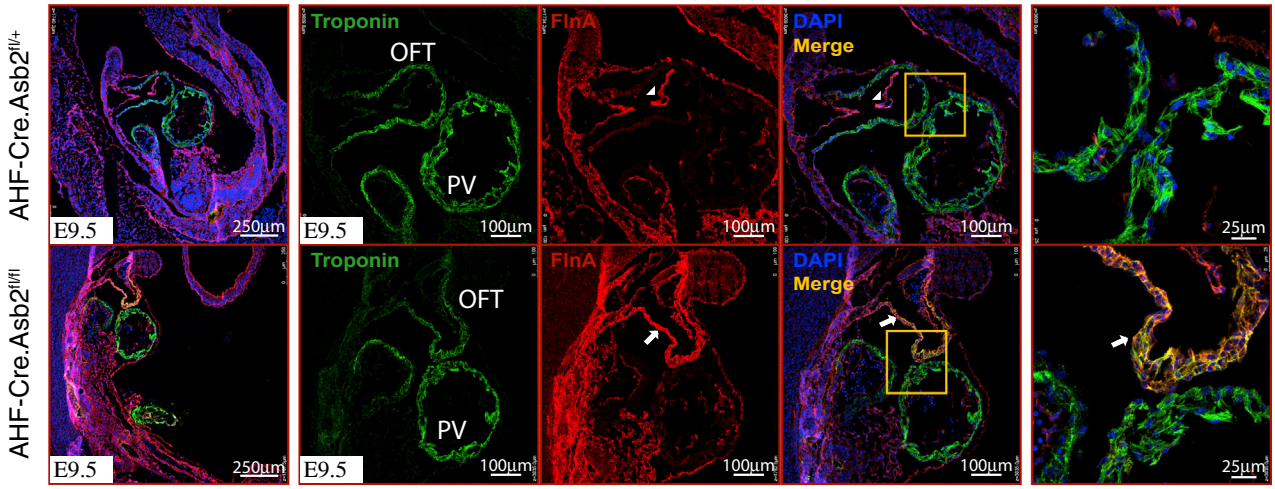

B

AHF-Cre.Asb2$^{fl/+}$ X Asb2$^{fl/fl}$

	Expected	Observed at P0.5
AHF^{Cre}Asb2$^{fl/fl}$	25%	0/29 (0%)
AHF^{Cre}Asb2$^{fl/+}$	25%	13/29 (44.8%)
Control	50%	16/29 (55.1%)

AHF-Cre.Asb2$^{fl/+}$ X Asb2$^{fl/fl}$.FlnA$^{fl/fl}$

		Expected	Observed at P0.5
AHF^{Cre}	Asb2$^{fl/fl}$.FlnA$^{fl/+}$	12.5%	1/31 (3.2%)
	Asb2$^{fl/fl}$.FlnA$^{fl/y}$	12.5%	**4/31 (12.9%)**
	Asb2$^{fl/+}$.FlnA$^{fl/+}$	12.5%	6/31 (19.3%)
	Asb2$^{fl/+}$.FlnA$^{fl/y}$	12.5%	6/31 (19.3%)
	Control	50%	14/31 (45.2%)

Dead at P0.5-1.5

Figure 5. Flna Removal from AHF^{Cre}.Asb2 Mutant Hearts Partially Rescues Their Lethality

(A) Immunohistochemistry on E9.5 AHF-Cre.Abs2 mutant hearts (AHF-Cre.Asb2$^{fl/fl}$, lower panel) and littermate controls (AHF-Cre.Asb2$^{fl/+}$, top panel) using Flna (red)- and Troponin-T (green)-specific antibodies. Note overexpression of Flna in the OFT (white arrows) of the AHF-Cre.Asb2 mutant hearts but not the primitive left ventricle (PV) that harbors normal Asb2 levels thus serving as an internal control. Flna expression in the control hearts is restricted to the endocardial layer (white arrow heads). Scale bar is equivalent to 250 μm in the first column (left); 100 μm in the second, third, and fourth columns; 25 μm in the fifth column (far right) as indicated.

(B) Table showing the survival of AHF-Cre.Asb2 mutant (top) and AHF-Cre.Asb2-Flna double mutant (bottom) mice. Note that no AHF-Cre.Abs2 mutant mice are observed at P0.5. However, the AHF-Cre.Asb2-Flna double mutant (Asb2$^{fl/fl}$.Flna$^{fl/y}$) mice are born at the expected Mendelian ratios. AHF-Cre.Asb2-mutant mice harboring one copy of Flna (Asb2$^{fl/fl}$.Flna$^{fl/+}$) are also born yet at lower percentage than what is expected by Mendelian genetics. These mice die, however, right after birth. P0.5, postnatal day 0.5.

Asb2 Removal from the Anterior Heart Field Leads to Double Outlet Right Ventricle) in Mice

To determine the cardiac defects of the AHF-Cre.Asb2$^{fl/fl}$.Flna$^{fl/+}$, we examined these mice at e16.5–e17.5 after the completion of cardiac morphogenesis but prior to the perinatal mortality associated with this genotype. Five litters were analyzed. Figure 6A shows the survival rate of these mice at E16.5. Gross examination of these hearts revealed that both the aorta and the pulmonary artery originate in the RV (Figure 6B, middle panel, yellow circle). In contrast, both the control hearts (Figure 6B, left panel) and those with AHF-Cre.Asb2-Flna double mutant (Figure 6B, right panel) were grossly normal with the pulmonary artery originating in the RV and the aorta originating in

A

AHF-Cre.Asb2$^{fl/+}$ X Asb2$^{fl/fl}$.FlnA$^{fl/fl}$

		Expected	Observed at E16.5
AHF-Cre.	Asb2$^{fl/fl}$.FlnA$^{fl/+}$	12.5%	5/51 (9.8%)
	Asb2$^{fl/fl}$.FlnA$^{fl/y}$	12.5%	5/51 (9.8%)
	Asb2$^{fl/+}$.FlnA$^{fl/+}$	12.5%	13/51 (25.5%)
	Asb2$^{fl/+}$.FlnA$^{fl/y}$	12.5%	7/51 (13.7%)
Control		50%	21/51 (41.2%)

B

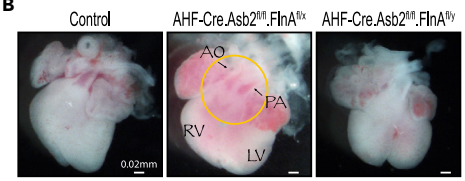

C

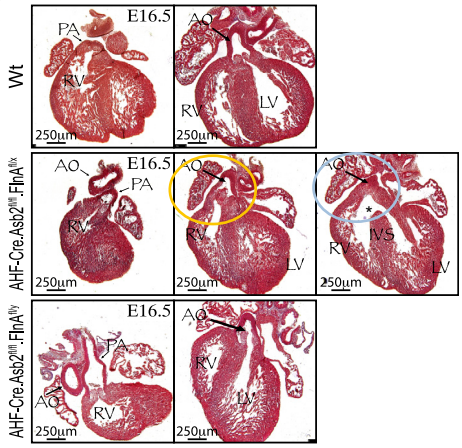

D

	Control	AHF-Cre.Asb2$^{fl/fl}$ FlnA$^{fl/x}$	AHF-Cre.Asb2$^{fl/fl}$ FlnA$^{fl/y}$
Normal	4/4	0/5	4/4
DORV/ VSD	0/4	5/5	0/4

Figure 6. AHF-Asb2 Mutant Hearts Have Double Outlet Right Ventricle and Ventricular Septal Defect

(A) Table showing the survival of AHF-Cre.Asb2-Flna double mutant mice at E16.5.

(B) E16.5 whole hearts of AHF-Cre.Asb2-mutant embryos with one copy of Flna (AHF-Cre.Asb2$^{fl/fl}$.Flna$^{fl/x}$), AHF-Cre.Asb2.Flna double mutants (AHF-Cre.Asb2$^{fl/fl}$.Flna$^{fl/fl}$), and wild-type control. Note that both the pulmonary artery (PA) and the aorta (Ao) are open in the right ventricle (RV) of the AHF-Cre.Asb2$^{fl/fl}$.Flna$^{fl/x}$ hearts (yellow circle). Scale bar is equivalent to 0.02 mm as indicated.

(C) Masson trichrome staining of E16.5 heart sections of control (Wt) (top), AHF-Cre.Asb2$^{fl/fl}$.Flna$^{fl/x}$ (middle), and AHF-Cre.Asb2$^{fl/fl}$.Flna$^{fl/fl}$ (bottom) embryos. Note that both the pulmonary artery and the aorta open in the right ventricle of the AHF-Cre.Asb2$^{fl/fl}$.Flna$^{fl/x}$ hearts (yellow circle, middle panel) but not the Wt or the AHF-Cre.Asb2$^{fl/fl}$.Flna$^{fl/fl}$ hearts. The AHF-Cre.Asb2$^{fl/fl}$.Flna$^{fl/x}$ also have a VSD indicated by asterisk (middle panel, right). Ao, aorta; PA, pulmonary artery; RV, right ventricle; LV, left ventricle; IVS, interventricular septum. Scale bar is equivalent to 250 μm.

(D) Number of E16.5 hearts with DORV in Wt, AHF-Cre.Asb2$^{fl/fl}$.Flna$^{fl/x}$, and AHF-Cre.Asb2$^{fl/fl}$.Flna$^{fl/fl}$ embryos. Note that 5/5 Asb2$^{fl/fl}$.Flna$^{fl/x}$ have DORV accompanied by a VSD suggesting 100% disease penetrance in these mice.

the LV. Serial sections of mutant and control hearts (Figure 6C) further confirm that the AHF-Cre.Asb2$^{fl/fl}$.Flna$^{fl/x}$ mice have DORV (Figure 6C middle panel, yellow oval). This is also accompanied by a ventricular septal defect (Figure 6C middle panel right, indicated by asterisk), a feature commonly associated with DORV in patients with congenital heart disease (Obler et al., 2008). As shown in Figure 6D, the DORV phenotype appeared to be fully penetrant in the AHF-Cre.Asb2$^{fl/fl}$.Flna$^{fl/x}$ hearts. Notably, the DORV phenotype is corrected in the AHF-Cre.Asb2-Flna double mutant hearts (AHF-Cre.Asb2$^{fl/fl}$.Flna$^{fl/y}$, Figure 6C lower panel).

Asb2 Is Required for Human Embryonic Stem Cell-Derived Cardiomyocyte Differentiation

To further investigate if the requirement for Asb2 for cardiac development is conserved during human cardiomyocyte differentiation, we turned to human embryonic stem cell (hESC)-derived cardiomyocyte *in vitro* differentiation. Both ASB2 variants 1 (Asb2β in mice) and 2 (Asb2α in mice) are expressed at different stages of cardiomyocyte differentiation (Figure 7A, top and bottom graphs, respectively). Using CRISPR/Cas9 genome editing technology, we then generated ASB2-null hESCs. The guides were designed in exon 2 (targeting variant 1 specifically) or exon 4 (targeting variants 1 and 2) (Figure S3A). Four wild-type (Wt) (received the CRISPR/Cas9 constructs but failed to generate an in/del) and four knockout (KO) lines were generated. The genotype of all lines was confirmed by sequencing (refer to Transparent Methods), and the knockouts were confirmed by qPCR (Figure 7B, right panel). Wt clones were able to differentiate into beating cardiomyocytes, whereas all four KO lines failed to do so (Video S2, top panels for Wt clones and bottom panels for KO clones). Calcium cycling was also impaired in the Asb2-null derived hESCs (Video S3, left panel for Wt and right panel for KO, and Figure S3B). Two Wt and two KO lines were used for further investigation. qPCR analysis on RNA from cardiomyocytes derived from these cells

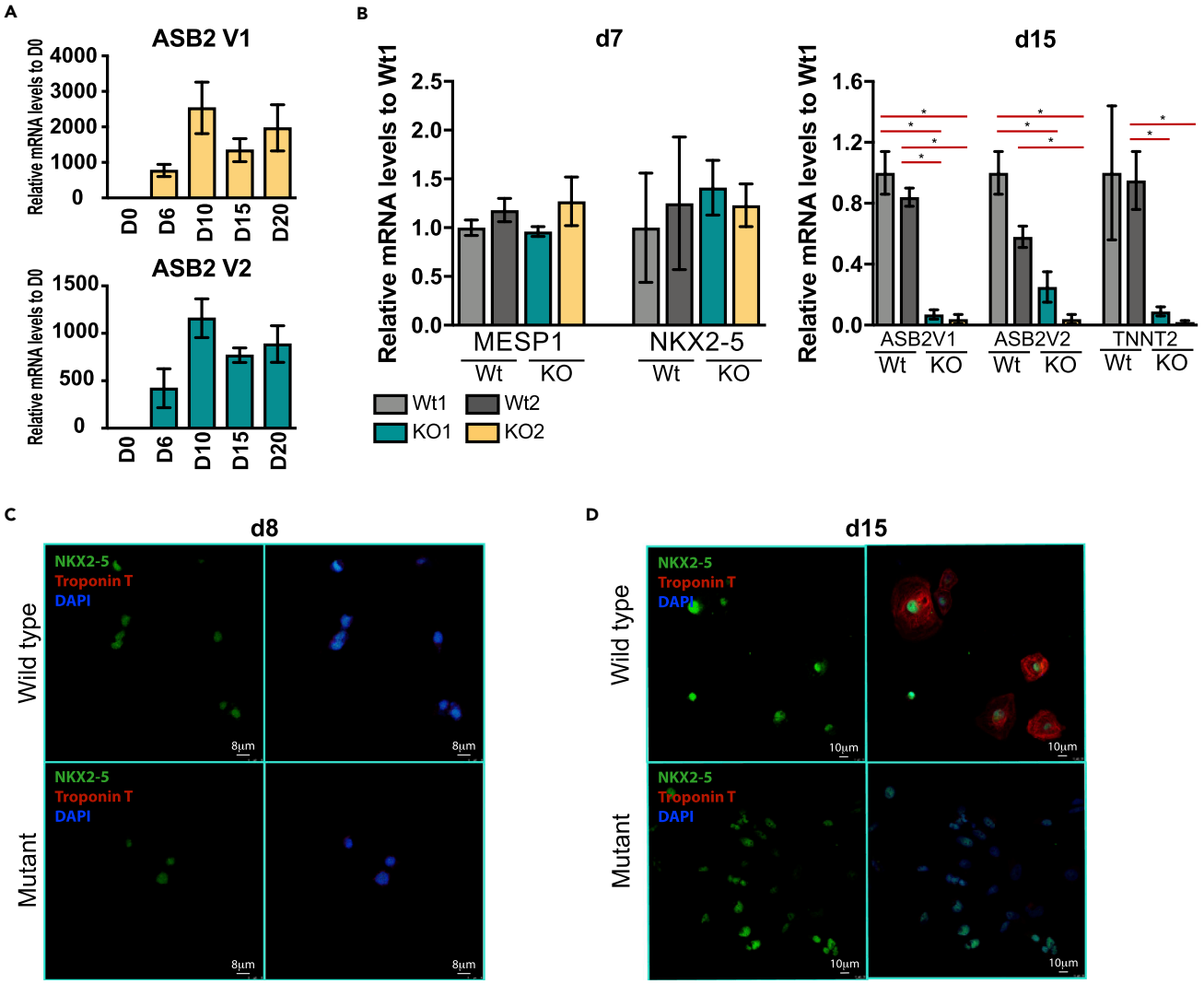

Figure 7. ASB2 Is Essential for Human Embryonic Stem Cell (hESC)-derived Cardiomyocytes Differentiation

(A) qPCR analysis of RNA from hESC-derived cardiomyocytes at different stages of differentiation. Note that both ASB2 variants are expressed at the different stages. N = 4 for D0, n = 5 for all other stages. Data are represented as mean ± SEM.

(B) qPCR analysis of RNA extracted from two different wild-type (Wt) clones and two ASB2 mutant (KO) clones d7 (left) and d15 (right) differentiated hESCs. Note reduced Troponin T (differentiation marker) transcripts in the mutants at d15 and no difference in MESP1 and NKX2-5 (cardiac progenitor markers) levels at d7. N = 3 per sample for d7 and N = 4 per sample for d14. Data are represented as mean ± SEM. * = $p < 0.05$. Two-way ANOVA was used for analysis using GraphPad Prism. $p < 0.05$ is considered statistically significant.

(C and D) Immunostaining of d8 (C) and d15 (D) differentiated Wt and ASB2 mutant cells (KO). Note reduced Troponin T (red)-positive mutant cells at d15 but no difference in NKX2-5 (green) levels between Wt and mutant cells at both stages. DAPI (blue) marks all nuclei. Scale bar is equivalent to 8 μm in (C) and 10 μm in (D) as indicated.

shows that cardiac Troponin T transcript levels (TNNT2, marker of cardiomyocyte differentiation) are greatly reduced in the KO lines at d15 of differentiation (Figure 7B, right). On the other hand, both NKX2-5 and MESP1 (markers of cardiac progenitors) are normally expressed at d7 of differentiation (Figure 7B, left). This was further confirmed at the protein level by immunostaining that shows great reduction in cardiac Troponin T (red) expression at d15 (Figure 7D) and normal NKX2-5 levels (green) at days 15 and 8 (Figures 7C and 7D, respectively). These data suggest that Asb2-null hES cells can commit to the cardiac lineage but arrest in differentiation prior to the generation of functional cardiomyocytes.

We then examined if ASB2 regulation of the TGFβ/SMAD signaling seen in mice hearts is conserved in the human cells. As discussed above, upon TGFβ/Smad activation, the signaling transducer Smad4 is

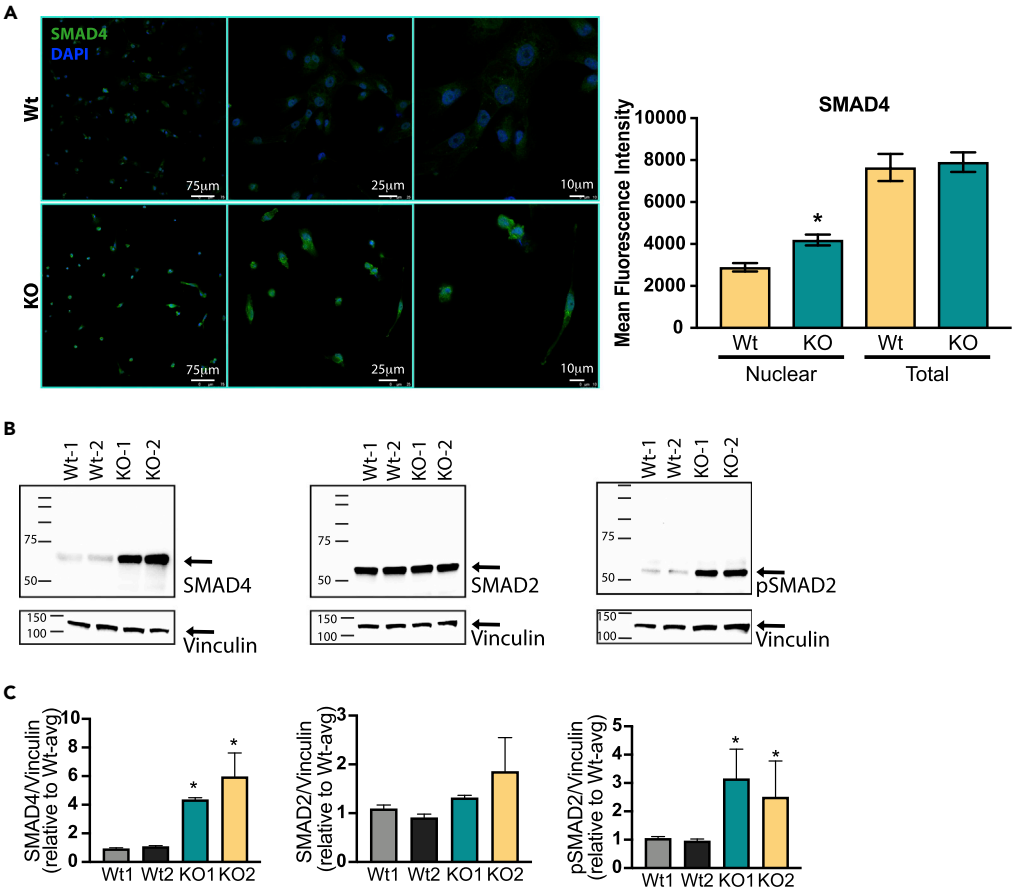

Figure 8. ASB2 Is an Upstream Regulator of TGFb/SMAD Pathway in hESC-derived Cardiomyocytes

(A) Immunostaining of d15 Wt and ASB2 mutant (KO) hESC-derived cardiomyocytes using SMAD4-specific antibody (green). Note reduced level of nuclear but not total mean fluorescence intensity of SMAD4-positive cells in the KOs (quantification graphs on the right). DAPI (blue) marks all nuclei. Scale bar is equivalent to 75 μm in the first column and 25 μm in the second and third columns as indicated. *: $p < 0.005$ significant versus Wt. Unpaired t test was used for analysis using GraphPad Prism.

(B and C) (B) Western blot analysis of Wt and ASB2 mutant (KO) hESC-derived cardiomyocytes using SMAD4, SMAD2, and pSMAD2 antibodies. Note increase of SMAD4 and pSMAD2 in the mutant clones. Data are representative of three separate experiments (C) Quantification of the western blot analysis in (B). Data are average of quantification from three separate experiments. *: significant versus Wt1 and Wt2. $p < 0.05$ is considered statistically significant. One-way ANOVA was used for analysis using GraphPad Prism.

translocated to the nucleus to activate downstream targets. Figure 8A shows an increase in nuclear SMAD4 (green) in the ASB2-null hES-derived cardiomyocytes. The nuclear versus total SMAD4 was quantified (Figure 8A, right graph) showing that nuclear SMAD4 signal is doubled in the ASB2-null cells, whereas total Smad4 levels remain the same. Western blot analysis on total protein extracts from these cells also confirms significant increase in both SMAD4 and pSMAD2 protein levels (Figures 8B and 8C). This further confirms that the TGFβ/SMAD signaling pathway is activated in Asb2-null cardiomyocytes.

DISCUSSION

In this study, we provide strong evidence for the role of Asb2 in controlling heart morphogenesis partly through its regulation of the actin-binding protein, Filamin A (Flna), and Tgfβ/Smad signaling. We further show that this regulation is part of the DORV disease pathogenesis.

Using CUBIC clearing technique combined with immunofluorescence and confocal microscopy, we show that the Asb2-mutant hearts have shorter heart tubes and do not form the fully looped helical structure. RNA-seq analysis also reveals that a number of genes that have been linked to cardiac looping defects

are altered in the Asb2-mutant hearts. Recent morphological analysis of Asb2 null embryos suggested that cardiac looping in the total body null is largely intact (Métais et al., 2018). To examine this more carefully, we exploited recent advances in tissue clearing coupled to optical sectioning and 3D reconstruction. This analysis of the intact embryos, however, allows us to refine these findings and to examine the Asb2 mutant hearts more thoroughly and at a slightly later point in development. Although the hearts do start to loop, they arrest early on before making it to the helical fully looped heart. Measurement of the heart tube length reveals shorter heart tubes in the mutant hearts, which could explain the inability of the heart to fully form the helical structure. These data further reveal the important role of Asb2 regulation of cardiomyocyte differentiation on the normal growth of the heart tube. We show that the CUBIC technique combined with immunofluorescence/confocal microscopy has distinct advantages over traditional morphological analysis for the phenotypic analysis of mouse embryos and allows for the detection of subtle phenotypes and morphological abnormalities.

Our data further reveal that Filamin A (Flna) is aberrantly overexpressed in the Asb2-mutant cardiomyocytes that normally do not express Flna protein. This is consistent with the data that Metais et al. reported. We also show that this regulation is dose dependent. We further show that Asb2-Flna regulate Tgfβ-Smad signaling. Nuclear pSmad2 is overexpressed in the Asb2-mutant hearts consistent with the upregulation of this signaling pathways. Its levels are restored to normal in the Asb2.Flna double mutants further showing that Asb2 regulates SMAD signaling through the Flna pathway. RNA-seq analysis also reveals that regulation of the Tgfβ-Smad pathway in the Asb2-mutant hearts and the Foxa genes, which are downstream effectors of the Tgfβ/Smad signaling (Tang et al., 2011), is in fact restored to normal in the Asb2-Flna double mutants. Flna has been previously shown to associate with Smad2 signaling (Sasaki et al., 2001). Moreover, Tgfβ/Smad2/3 signaling is impaired in the multivalve degeneration disorder, X-linked myxomatous valvular dystrophy, in which FLNA mutations were reported (Geirsson et al., 2012; Norris et al., 2010). Our data provide further evidence for regulation of the Tgfβ/Smad cycle by Flna and show that Asb2 is upstream of this regulatory pathway in the developing heart.

Using human embryonic stem cell (hESC)-derived cardiomyocytes, we further show that the Asb2 role in embryonic heart differentiation is conserved in humans. Although ASB2-null hESCs are able to form cardiac progenitor cells (marked by expression of MESP1 and NKX2-5), they have an impaired ability to differentiate into beating TNNT+ cardiomyocytes. It is important to note here that the difference between Troponin T levels in the Asb2-null hESCs and the Asb2 mutants *in vivo* could be due to the total knockout in the cells that is more severe than the conditional *in vivo* knockout. Additionally, the cell system lacks signaling coming from the endocardium, which could also explain this difference. These results demonstrate that, in human PSCs differentiating *in vitro*, ASB2-mediated targeted degradation is required for the differentiation from NKX2-5+ progenitors to beating TNNT+ cardiomyocytes and that deletion of ASB2 results in a differentiation arrest at the progenitor stage. Moreover, the finding that these cells have increased levels of SMAD4 and pSMAD2, markers of TGFβ/SMAD pathway activation, provides further evidence that ASB2 is an upstream regulator of the TGFβ/SMAD pathway during the differentiation of human cardiomyocytes. These considerations become increasingly important given the potential of pluripotent stem cell-derived CMs to serve as a renewable cell source for cardiac regeneration in the injured heart.

Given that Flna is a direct target of Asb2 that is aberrantly upregulated in Asb2-mutant cardiomyocytes, we then investigated whether Asb2 cardiac mutant embryonic lethality can be rescued by the concurrent deletion of Flna. Accordingly, we generated AHF-Cre.Asb2$^{fl/fl}$.Flna$^{fl/y}$ double mutants. Our data show that, as opposed to the AHF-Cre.Asb2$^{fl/fl}$ single mutants that die by E11.5, the AHF-Cre.Asb2$^{fl/fl}$.Flna$^{fl/y}$ double mutants are born with the expected Mendelian ratios (Figure 5B) but die shortly after birth. This suggests partial rescue of lethality seen in the AHF-Cre.Asb2$^{fl/fl}$ mutant hearts. Of note, we also generated Nkx2-5$^{+/Cre}$.Asb2$^{fl/fl}$.Flna$^{fl/Y}$ double mutants that did not rescue the Asb2 lethality (Figure S2A), suggesting a greater Asb2 dependency or a more complex phenotype in these mice. These findings are not surprising owing to earlier and broader expression domain of the Nxk2-5^{Cre} compared with the AHF-Cre line. Moreover, AHF-Asb2-mutant mice with one Flna allele (AHF-Cre.Asb2$^{fl/fl}$.Flna$^{fl/x}$) sometimes also survive to P0, albeit at significantly lower than expected ratios (Figure 5B). Not only do these results suggest a dose dependency of Asb2 and its target Flna but they also allow us to identify DORV associated with ventricular septal defect (VSD) as a penetrant cardiac phenotype. More interestingly, this phenotype was rescued when Flna was abrogated by the concurrent deletion of Flna showing that both Asb2 and Flna play a functional role in the pathogenesis of DORV.

During cardiac development, the heart first forms as a primitive heart tube that then elongates and starts to loop by addition of cells from the anterior, posterior, and second heart field at both the venous and arterial poles. At the onset of looping, left-right asymmetry in the heart becomes morphologically evident and any defects in this process can lead to complex congenital heart problems, including DORV and VSDs (Ramsdell, 2005). The heart is the first organ to break the left-right symmetry in the developing embryo, and it has been shown that the actin-cytoskeleton is fundamental for laterality and modulation associated with heart looping. It was shown to provide the built-in mechanism required for cells to acquire left-right asymmetry (Linask and Vanauker, 2007; Tee et al., 2015). Abnormalities in the control of construction of the cytoskeleton has been previously shown to result in looping defects and ultimately lead to congenital heart problems (Langdon et al., 2012; Linask and Vanauker, 2007). Our data and the data from Metais et al. provide solid evidence for the Asb2-Flna regulation of the actin cytoskeleton during heart morphogenesis (Métais et al., 2018). Our data extend this regulation to show that it is important for normal heart tube and OFT development and, if perturbed, leads to DORV and VSD in the developing mammalian heart. Additionally, we suggest a mechanism where Asb2 downregulation leads to abnormal overexpression of Flna that ultimately leads to increased activity of the Tgfβ/Smad2 signaling in the myocardium thus causing growth/elongation defects and DORV in the mammalian heart. Indeed, prior reports have implicated the Tgfβ superfamily and Smad2/3 in left-right asymmetry, and Tgfβ2 mutant mice have been shown to develop DORV and die right after birth (Azhar et al., 2003; Sanford et al., 1997; Whitman and Mercola, 2001). In humans, a missense mutation in Flna (c.5290G>A (p.A1764T) has been reported in a patient with DORV (de Wit et al., 2011). Since missense mutations can result in both loss and gain of function, future studies will be required to determine the effect of this mutation on Flna expression and function. Thus, our data demonstrate a link between targeted protein turnover and the development of DORV and highlights the potential of the ASB2/FLNA axis as a diagnostic, prognostic, and/or therapeutic target for patients with DORV.

Limitations of the Study

Although our data show that the role of Asb2 in heart morphogenesis is conserved between mice and human, a limitation is that the *in vivo* murine system is a conditional knockout compared with the total knockout in the human cells system. Additionally, as we know, a cross talk between the endocardium and the myocardium occurs during heart morphogenesis, and this again is lacking in our human cell system.

METHODS

All methods can be found in the accompanying Transparent Methods supplemental file.

DATA AND CODE AVAILABILITY

RNA-seq data have been deposited in NCBI's Gene Expression Omnibus (GEO). The accession number for the RNA-seq data reported in this paper is GEO: GSE145495.

SUPPLEMENTAL INFORMATION

Supplemental Information can be found online at https://doi.org/10.1016/j.isci.2020.100959.

ACKNOWLEDGMENTS

We thank all members of the Domian Lab for valuable insight and suggestions. We also thank the histology core at Dana Farber Cancer Institute/Harvard Medical School and the NextGen Sequencing core at Massachusetts General Hospital for technical support. This work was supported by the American Heart Association (17GRNT33630170), the Centre National de la Recherche Scientifique, and the University of Toulouse. A.Y. is a recipient of the Fund for Medical Discovery (FMD) Award from the Massachusetts General Hospital/Harvard Medical School.

AUTHOR CONTRIBUTIONS

Conceptualization, A.Y. and I.J.D.; Methodology, A.Y. and I.J.D.; Investigation A.Y., D.H., N.M., J.W.B., and S.D.; Writing – Original Draft, A.Y.; Writing – Review & Editing, A.Y., P.G.L., C.M.-L, P.T.L., and I.J.D.; Visualization, A.Y.; Supervision, A.Y. and I.J.D.; Funding Acquisition, A.Y. and I.J.D.

DECLARATION OF INTERESTS

The authors declare no competing interests.

Received: August 16, 2019
Revised: December 17, 2019
Accepted: February 26, 2020
Published: March 27, 2020

REFERENCES

Azhar, M., Schultz, J.E.J., Grupp, I., Dorn, G.W., Meneton, P., Molin, D.G.M., Gittenberger-de Groot, A.C., and Doetschman, T. (2003). Transforming growth factor beta in cardiovascular development and function. Cytokine Growth Factor Rev. *14*, 391–407.

Bardot, E., Calderon, D., Santoriello, F., Han, S., Cheung, K., Jadhav, B., Burtscher, I., Artap, S., Jain, R., Epstein, J., et al. (2017). Foxa2 identifies a cardiac progenitor population with ventricular differentiation potential. Nat. Commun. *8*, 14428.

Bello, N.F., Lamsoul, I., Heuzé, M.L., Métais, A., Moreaux, G., Calderwood, D.A., Duprez, D., Moog-Lutz, C., and Lutz, P.G. (2009). The E3 ubiquitin ligase specificity subunit ASB2beta is a novel regulator of muscle differentiation that targets filamin B to proteasomal degradation. Cell Death Differ. *16*, 921–932.

Bruneau, B.G. (2008). The developmental genetics of congenital heart disease. Nature *451*, 943–948.

Bulteau, A.L., Lundberg, K.C., Humphries, K.M., Sadek, H.A., Szweda, P.A., Friguet, B., and Szweda, L.I. (2001). Oxidative modification and inactivation of the proteasome during coronary occlusion/reperfusion. J. Biol. Chem. *276*, 30057–30063.

Chen, J.N., van Eeden, F.J., Warren, K.S., Chin, A., Nüsslein-Volhard, C., Haffter, P., and Fishman, M.C. (1997). Left-right pattern of cardiac BMP4 may drive asymmetry of the heart in zebrafish. Development *124*, 4373–4382.

Davey, J.R., Watt, K.I., Parker, B.L., Chaudhuri, R., Ryall, J.G., Cunningham, L., Qian, H., Sartorelli, V., Sandri, M., Chamberlain, J., et al. (2016). Integrated expression analysis of muscle hypertrophy identifies Asb2 as a negative regulator of muscle mass. JCI Insight *1*, https://doi.org/10.1172/jci.insight.85477.

de Wit, M.C.Y., de Coo, I.F.M., Lequin, M.H., Halley, D.J.J., Roos-Hesselink, J.W., and Mancini, G.M.S. (2011). Combined cardiological and neurological abnormalities due to filamin A gene mutation. Clin. Res. Cardiol. *100*, 45–50.

de Wit, M.C.Y., Kros, J.M., Halley, D.J.J., de Coo, I.F.M., Verdijk, R., Jacobs, B.C., and Mancini, G.M.S. (2009). Filamin A mutation, a common cause for periventricular heterotopia, aneurysms and cardiac defects. J. Neurol. Neurosurg. Psychiatry *80*, 426–428.

Domian, I.J., Chiravuri, M., van der Meer, P., Feinberg, A.W., Shi, X., Shao, Y., Wu, S.M., Parker, K.K., and Chien, K.R. (2009). Generation of functional ventricular heart muscle from mouse ventricular progenitor cells. Science *326*, 426–429.

Fan, Y., Xie, P., Zhang, T., Zhang, H., Gu, D., She, M., and Li, H. (2008). Regulation of the stability and transcriptional activity of NFATc4 by ubiquitination. FEBS Lett. *582*, 4008–4014.

Feng, Y., Chen, M.H., Moskowitz, I.P., Mendonza, A.M., Vidali, L., Nakamura, F., Kwiatkowski, D.J., and Walsh, C.A. (2006). Filamin A (FLNA) is required for cell-cell contact in vascular development and cardiac morphogenesis. Proc. Natl. Acad. Sci. U S A *103*, 19836–19841.

Fujita, M., Mitsuhashi, H., Isogai, S., Nakata, T., Kawakami, A., Nonaka, I., Noguchi, S., Hayashi, Y.K., Nishino, I., and Kudo, A. (2012). Filamin C plays an essential role in the maintenance of the structural integrity of cardiac and skeletal muscles, revealed by the medaka mutant zacro. Dev. Biol. *361*, 79–89.

Fukuda, R., Gunawan, F., Beisaw, A., Jimenez-Amilburu, V., Maischein, H.-M., Kostin, S., Kawakami, K., and Stainier, D.Y.R. (2017). Proteolysis regulates cardiomyocyte maturation and tissue integration. Nat. Commun. *8*, 14495.

Geirsson, A., Singh, M., Ali, R., Abbas, H., Li, W., Sanchez, J.A., Hashim, S., and Tellides, G. (2012). Modulation of transforming growth factor-β signaling and extracellular matrix production in myxomatous mitral valves by angiotensin II receptor blockers. Circulation *126*, S189–S197.

Glickman, M.H., and Ciechanover, A. (2002). The ubiquitin-proteasome proteolytic pathway: destruction for the sake of construction. Physiol. Rev. *82*, 373–428.

Guibal, F.C., Moog-Lutz, C., Smolewski, P., Di Gioia, Y., Darzynkiewicz, Z., Lutz, P.G., and Cayre, Y.E. (2002). ASB-2 inhibits growth and promotes commitment in myeloid leukemia cells. J. Biol. Chem. *277*, 218–224.

Heuzé, M.L., Lamsoul, I., Baldassarre, M., Lad, Y., Lévêque, S., Razinia, Z., Moog-Lutz, C., Calderwood, D.A., and Lutz, P.G. (2008). ASB2 targets filamins A and B to proteasomal degradation. Blood *112*, 5130–5140.

Hu, D., Linders, A., Yamak, A., Correia, C., Kijlstra, J.D., Garakani, A., Xiao, L., Milan, D.J., van der Meer, P., Serra, M., et al. (2018). Metabolic maturation of human pluripotent stem cell-derived cardiomyocytes by inhibition of HIF1α and LDHA. Circ. Res. *123*, 1066–1079.

Jung, T., Catalgol, B., and Grune, T. (2009). The proteasomal system. Mol. Aspects Med. *30*, 191–296.

Kedar, V., McDonough, H., Arya, R., Li, H.-H., Rockman, H.A., and Patterson, C. (2004). Muscle-specific RING finger 1 is a bona fide ubiquitin ligase that degrades cardiac troponin I. Proc. Natl. Acad. Sci. U S A *101*, 18135–18140.

Kolesová, H., Čapek, M., Radochová, B., Janáček, J., and Sedmera, D. (2016). Comparison of different tissue clearing methods and 3D imaging techniques for visualization of GFP-expressing mouse embryos and embryonic hearts. Histochem. Cell Biol. *146*, 141–152.

Kyndt, F., Gueffet, J.-P., Probst, V., Jaafar, P., Legendre, A., Le Bouffant, F., Toquet, C., Roy, E., McGregor, L., Lynch, S.A., et al. (2007). Mutations in the gene encoding filamin A as a cause for familial cardiac valvular dystrophy. Circulation *115*, 40–49.

Laine, A., and Ronai, Z. (2005). Ubiquitin chains in the ladder of MAPK signaling. Sci. STKE *2005*, re5.

Langdon, Y., Tandon, P., Paden, E., Duddy, J., Taylor, J.M., and Conlon, F.L. (2012). SHP-2 acts via ROCK to regulate the cardiac actin cytoskeleton. Development *139*, 948–957.

Le Garrec, J.-F., Domínguez, J.N., Desgrange, A., Ivanovitch, K.D., Raphaël, E., Bangham, J.A., Torres, M., Coen, E., Mohun, T.J., and Meilhac, S.M. (2017). A predictive model of asymmetric morphogenesis from 3D reconstructions of mouse heart looping dynamics. Elife *6*, https://doi.org/10.7554/eLife.28951.

Li, J., Horak, K.M., Su, H., Sanbe, A., Robbins, J., and Wang, X. (2011). Enhancement of proteasomal function protects against cardiac proteinopathy and ischemia/reperfusion injury in mice. J. Clin. Invest. *121*, 3689–3700.

Linask, K.K., and Vanauker, M. (2007). A role for the cytoskeleton in heart looping. ScientificWorldJournal *7*, 280–298.

Lombardi, R., Dong, J., Rodriguez, G., Bell, A., Leung, T.K., Schwartz, R.J., Willerson, J.T., Brugada, R., and Marian, A.J. (2009). Genetic fate mapping identifies second heart field progenitor cells as a source of adipocytes in arrhythmogenic right ventricular cardiomyopathy. Circ. Res. *104*, 1076–1084.

Männer, J. (2009). The anatomy of cardiac looping: a step towards the understanding of the morphogenesis of several forms of congenital cardiac malformations. Clin. Anat. *22*, 21–35.

Martinsen, B.J., and Lohr, J.L. (2015). Cardiac development. In Handbook of Cardiac Anatomy, Physiology, and Devices, P.A. Laizzo, ed. (Springer), pp. 23–33.

Mercola, M., Ruiz-Lozano, P., and Schneider, M.D. (2011). Cardiac muscle regeneration: lessons from development. Genes Dev. *25*, 299–309.

Métais, A., Lamsoul, I., Melet, A., Uttenweiler-Joseph, S., Poincloux, R., Stefanovic, S., Valière, A., Gonzalez de Peredo, A., Stella, A., Burlet-Schiltz, O., et al. (2018). Asb2α-filamin A axis is essential for actin cytoskeleton remodeling during heart development. Circ. Res. *122*, e34–e48.

Mine, N., Anderson, R.M., and Klingensmith, J. (2008). BMP antagonism is required in both the node and lateral plate mesoderm for mammalian left-right axis establishment. Development *135*, 2425–2434.

Murdaca, J., Treins, C., Monthouël-Kartmann, M.-N., Pontier-Bres, R., Kumar, S., Van Obberghen, E., and Giorgetti-Peraldi, S. (2004). Grb10 prevents Nedd4-mediated vascular endothelial growth factor receptor-2 degradation. J. Biol. Chem. *279*, 26754–26761.

Nemer, M. (2008). Genetic insights into normal and abnormal heart development. Cardiovasc. Pathol. *17*, 48–54.

Norris, R.A., Moreno-Rodriguez, R., Wessels, A., Merot, J., Bruneval, P., Chester, A.H., Yacoub, M.H., Hagège, A., Slaugenhaupt, S.A., Aikawa, E., et al. (2010). Expression of the familial cardiac valvular dystrophy gene, filamin-A, during heart morphogenesis. Dev. Dyn. *239*, 2118–2127.

Obler, D., Juraszek, A.L., Smoot, L.B., and Natowicz, M.R. (2008). Double outlet right ventricle: aetiologies and associations. J. Med. Genet. *45*, 481–497.

Pagan, J., Seto, T., Pagano, M., and Cittadini, A. (2013). Role of the ubiquitin proteasome system in the heart. Circ. Res. *112*, 1046–1058.

Powell, S.R., Davies, K.J.A., and Divald, A. (2007). Optimal determination of heart tissue 26S-proteasome activity requires maximal stimulating ATP concentrations. J. Mol. Cell. Cardiol. *42*, 265–269.

Ramsdell, A.F. (2005). Left-right asymmetry and congenital cardiac defects: getting to the heart of the matter in vertebrate left-right axis determination. Dev. Biol. *288*, 1–20.

Ribeiro, I., Kawakami, Y., Büscher, D., Raya, A., Rodríguez-León, J., Morita, M., Rodríguez Esteban, C., and Izpisúa Belmonte, J.C. (2007). Tbx2 and Tbx3 regulate the dynamics of cell proliferation during heart remodeling. PLoS One *2*, e398.

Sanford, L.P., Ormsby, I., Gittenberger-de Groot, A.C., Sariola, H., Friedman, R., Boivin, G.P., Cardell, E.L., and Doetschman, T. (1997). TGFbeta2 knockout mice have multiple developmental defects that are non-overlapping with other TGFbeta knockout phenotypes. Development *124*, 2659–2670.

Sasaki, A., Masuda, Y., Ohta, Y., Ikeda, K., and Watanabe, K. (2001). Filamin associates with Smads and regulates transforming growth factor-beta signaling. J. Biol. Chem. *276*, 17871–17877.

Shi, Y., and Massagué, J. (2003). Mechanisms of TGF-beta signaling from cell membrane to the nucleus. Cell *113*, 685–700.

Spaich, S., Will, R.D., Just, S., Spaich, S., Kuhn, C., Frank, D., Berger, I.M., Wiemann, S., Korn, B., Koegl, M., et al. (2012). F-box and leucine-rich repeat protein 22 is a cardiac-enriched F-box protein that regulates sarcomeric protein turnover and is essential for maintenance of contractile function in vivo. Circ. Res. *111*, 1504–1516.

Spinner, C.A., Uttenweiler-Joseph, S., Metais, A., Stella, A., Burlet-Schiltz, O., Moog-Lutz, C., Lamsoul, I., and Lutz, P.G. (2015). Substrates of the ASB2α E3 ubiquitin ligase in dendritic cells. Sci. Rep. *5*, 16269.

Srivastava, D. (2006). Making or breaking the heart: from lineage determination to morphogenesis. Cell *126*, 1037–1048.

Tainaka, K., Kubota, S.I., Suyama, T.Q., Susaki, E.A., Perrin, D., Ukai-Tadenuma, M., Ukai, H., and Ueda, H.R. (2014). Whole-body imaging with single-cell resolution by tissue decolorization. Cell *159*, 911–924.

Tang, Y., Shu, G., Yuan, X., Jing, N., and Song, J. (2011). FOXA2 functions as a suppressor of tumor metastasis by inhibition of epithelial-to-mesenchymal transition in human lung cancers. Cell Res. *21*, 316–326.

Tee, Y.H., Shemesh, T., Thiagarajan, V., Hariadi, R.F., Anderson, K.L., Page, C., Volkmann, N., Hanein, D., Sivaramakrishnan, S., Kozlov, M.M., and Bershadsky, A.D. (2015). Cellular chirality arising from the self-organization of the actin cytoskeleton. Nat. Cell Biol. *17*, 445–457.

Valdés-Mas, R., Gutiérrez-Fernández, A., Gómez, J., Coto, E., Astudillo, A., Puente, D.A., Reguero, J.R., Álvarez, V., Morís, C., León, D., et al. (2014). Mutations in filamin C cause a new form of familial hypertrophic cardiomyopathy. Nat. Commun. *5*, 5326.

van der Flier, A., and Sonnenberg, A. (2001). Structural and functional aspects of filamins. Biochim. Biophys. Acta *1538*, 99–117.

Vincentz, J.W., Barnes, R.M., and Firulli, A.B. (2011). Hand factors as regulators of cardiac morphogenesis and implications for congenital heart defects. Birth Defects Res. A Clin. Mol. Teratol. *91*, 485–494.

Whitman, M., and Mercola, M. (2001). TGF-beta superfamily signaling and left-right asymmetry. Sci. STKE *2001*, re1.

Yamak, A., and Nemer, M. (2015). Role of embryonic and differentiated cells in cardiac development. In Biomaterials for Cardiac Regeneration, E.J. Suuronen and M. Ruel, eds. (Springer), pp. 37–70.

Zhou, A.-X., Toylu, A., Nallapalli, R.K., Nilsson, G., Atabey, N., Heldin, C.-H., Borén, J., Bergo, M.O., and Akyürek, L.M. (2011). Filamin a mediates HGF/c-MET signaling in tumor cell migration. Int. J. Cancer *128*, 839–846.

iScience, Volume *23*

Supplemental Information

Loss of Asb2 Impairs Cardiomyocyte Differentiation and Leads to Congenital Double Outlet Right Ventricle

Abir Yamak, Dongjian Hu, Nikhil Mittal, Jan W. Buikema, Sheraz Ditta, Pierre G. Lutz, Christel Moog-Lutz, Patrick T. Ellinor, and Ibrahim J. Domian

Supplementary Data

Transparent Methods

Animals. All animal experimentations were carried out in accordance with institutional guidelines for animal care. Experiments were approved by the Massachusetts General Hospital's Subcommittee on Research Animal Care (SRAC), which serves as the Institutional Animal Care and Use Committee (IACUC) as required by the Public Health Service (PHS) Policy on Humane Welfare Regulations. The program and facilities have been fully accredited by the American Association for the Accreditation of Laboratory Animal Care (AAALAC) since July 30, 1993. The institutional assurance number with the Office for Protection from Research Risks at the N.I.H. is DI6-00361. All mice lines were kept on a C57BL/6 background. Approximately, 20 AHF-Cre, 20 Nkx2-5$^{+/Cre}$, 100 Asb2$^{fl/fl}$ and 100 Asb2$^{fl/fl}$.Flna$^{fl/fl}$ mice were used. To isolate embryos from pregnant females, cervical dislocation was used for euthanasia which is required for embryo collection in mice. Sex of the embryos was not an influence in this study due to the very early developmental stage. Embryos were analyzed at E8.5, E9.5, E10.5, and E11.5 as indicated in the results section where applicable. For the double outlet right ventricle analysis, hearts of E16.5 embryos were used.

Generation of Asb2 and Flna knockout embryos. Asb2$^{fl/fl}$ or Asb2$^{fl/fl}$.Flna$^{fl/fl}$ females were mated with Nkx2-5$^{+/Cre}$ or AHF-Cre male mice and plugs were checked on a daily basis. The day a plug is seen is considered embryonic day e0.5. Asb2$^{fl/fl}$, Flna$^{fl/fl}$, Nkx2-5$^{+/Cre}$ and AHF-Cre mice are previously described (Lamsoul et al., 2013; Lombardi et al., 2009; Pinto et al., 2014). Mice genotypes (adult and embryos) were determine by PCR genotyping. Genotyping oligos used are: Flna flox: 5' TCT TCC TCT TTC AGC TGG 3'and 5' ACA ACT GCT GCT CCA GAG 3'; Asb2 flox: 5' CAGTGTCTGCTCTGAGGTCTCTC 3' and 5' CAATCTCTCCCTGGTAGAAACAGTTTGG 3'; Nkx2-5 Cre: 5' GATTAGCTTAAGCGGAGCTGGGTGTCC 3' and 5' GCCGCATAACCAGTGAAACAGCATTGC 3'; AHF-Cre: 5' CCAGGCAAAGGCAAGAATAA 3' and 5' ATGTTTAGCTGGCCCAAATG 3'.

Immunohistochemistry. Immunofluorescence was done as previously described (Domian et al., 2009)**.** Tissues were permeabilized with 0.3% Triton and antigen retrieval was done using citrate buffer. Tissues were blocked with goat or donkey serum and primary antibodies were incubated overnight at 4^{o}C. Secondary antibodies linked to appropriate alexa fluor were incubated for 1 hour at room temperature. Excess antibodies were washed with Phosphate buffer saline with 0.2% tween-20. Tissues were mounted with prolong gold anti-fade mounting media. Antibodies used were: Asb2 (Abcam, ab13710); Filamin a (Abcam, ab76289); Nkx2-5 (Invitrogen, PA5-49431); pSmad2(Millipore, AB3849); Troponin T (Thermo-Scientific, MA5-12960; SMAD4 (Proteintech, 10231-1-AP). Masson Trichrome Staining was done on paraffin heart sections using the American Mastertech Scientific kit (Item No. KTMTR) according to the manufacturer's protocol. Paraffin sections were deparaffinized with 3 rounds of xylene followed by rehydration with serial dilutions of ethanol baths prior to staining. Outflow tract measurements were done on 2D images using ImageJ. The landmarks used for measurement are as shown in supplementary figure 1D.

CUBIC clearing and Immunostaining. Embryos were immersed in CUBIC-1 solution (25% urea, 15% TritonX-100, 25% N,N,N,N-tetrakis(2-hydroxypropyl)ethyl-enediamine) at 37^{o}C with gentle shaking till efficiently cleared (2-5 days depending on developmental stage). Following clearing, embryos were washed thoroughly with PBS and stained with Troponin T and/or Filamin A antibodies for 4-5 days (at 4^{o}C), washed with PBS and then incubated with the corresponding secondary antibodies coupled to Alexa Fluor 488 or 546 for additional 3-4 days (at 4^{o}C). DAPI was added to CUBIC-1 solution and the following PBS washes to mark nuclei. Following staining, embryos were then cleared with CUBIC-2 solution (50% sucrose, 25% urea and 10% 2,2',2'-nitrilotriethanol) for 1-2 days at 37^{o}C with gentle shaking and then immediately transferred to immersion oil and imaged with laser confocal microscopy (Leica TCS SP8). 90-120 z-stacks were taken for each embryo that were then used to generate the 3D reconstructions using either the Leica software or image J. The 3D images were then further analyzed for phenotypic defects. At least 5 embryos were analyzed for each condition. The clearing/staining technique was adapted from the established protocol by Kolesova *et al* (Kolesová et al., 2016). Heart tube measurements were done on 3D images

using ImageJ. The landmarks used for measuring the tube's length are as described in Le Garrec *et al* paper (Le Garrec et al., 2017).

RNA Extraction and qPCR. RNA extraction was done using the Qiagen RNeasy Micro Kit (Cat No. 74004) according to the manufacturer's protocol. qPCR analysis was done using the Applied Biosystems PowerUp SYBR Green Master mix (Cat No. A25742) according to manufacturer's protocol. Oligos used were: msAsb2α: 5' GCTCTGTTTCACTCTGGCTCT 3' and 5' CTTCAGCACGGGGTCCATAG 3'; msAsb2β: 5' AACCACCAGCCAGGACATTT 3' and 5' ACTTCTGCATGACCCCTTGG 3'; huASB2V1: 5' ATTGGGCAGGAGGAGTACAG 3' and 5' AACTCTCAGGAGGTGCAGT 3'; huASB2V2: 5' ATGACCCGCTTCTCCTATGC 3' and 5' CGAACTCTCAGGAGGTGCAG 3'. huTNNT2: 5' ACTTGGAGGCAGAGAAGTTCG 3' and 5' CCCGGTGACTTTAGCCTTCC 3'; huNKX2-5: 5' CGCACAGCTCTTTCTTTTCGG 3' and 5' CGCCTTCTATCCACGTGCC 3'; huMESP1: 5' CTTTTTGGCCTCAGCACCTTC 3' and 5' AGTGTCTAGCCCTATGGGTCC 3'.

RNA Sequencing. RNA was extracted from e9.5 embryo hearts using the Qiagen RNeasy Micro Kit (Cat No. 74004) and sent to the MGH Next Generation sequencing core. The libraries were sequenced using illumina HiSeq platform. Splice-aware alignment program STAR was used to map the sample sequencing reads to the *Mus musculus* mm10 reference genome. Gene expression counts were calculated using HTSeq based on current Ensembl annotation for mm10. The R package "edgeR" was then employed to make differential gene expression calls. Pathway analyses were done using "MetaCore-Clarivate" and "Ingenuity Pathway Analysis-Qiagen" softwares.

Human Pluripotent Stem Cell Culture and Differentiation. HUES9 hESC line (NIH Human Embryonic Stem Cell Registry Number 0022, generated by HSCI iPS Core at Harvard University) was used in generating CRISPR KO cell line. hESC culture, differentiation and dissociation protocols were based on previously published works (Hu et al., 2018). Briefly, hESCs were cultured in Essential 8 Medium (Thermo Fisher Scientific, MA) in Matrigel (BD Biosciences) coated cell culture plates. hESCs were differentiated in RPMI GlutaMAX (Thermo Fisher Scientific, MA) plus Gem21 NeuroPlex Serum-Free Supplement without insulin (Gemini Bio Products, CA) for the first 5 days. Small molecules CHIR99021 (STEMCELL Technologies, Vancouver, Canada) and IWP-4 (STEMCELL Technologies, Vancouver, Canada) were added on day 1 and 3, respectively. Differentiation media was then switched to RPMI GlutaMAX plus Gem21 NeuroPlex Serum-Free Supplement from day 7 to 10. Differentiating hESCs then underwent glucose starvation for 6 days, which resulted in highly pure populations of beating CMs.

hESC-CMs were re-plated onto Matrigel coated PDMS plates for confocal imaging. Imaging procedure and analysis were done based on previously published methods (Kijlstra et al., 2015). Briefly, Fluo-4, AM (Thermo Fisher Scientific, MA) calcium indicator were incubated with hESC-CMs prior to imaging. Movies of CMs at randomly selected regions were acquired in both DIC and GFP channels at 50 frames per second for 10 seconds. Calcium transients were analyzed using ImageJ software.

In vitro differentiation of the SHF-dsRed/Nkx2.5-eGFP cells was done as previously described (Domian et al., 2009).

Generation of ASB2-null hESCs. We used CRISPR/Cas9 genome editing technology to generate the ASB2-null hESCs according to the described protocol (Ran et al., 2013). Guide RNAs (gRNAs) specific for hASB2 variant 1 (equivalent to Asb2β in mouse) and those common for both variants 1 & 2 (mouse Asb2β & α respectively) were designed using CRISPR design online tool, cloned into CRISPR/Cas9-GFP plasmid backbone (pSpCas9 from Addgene) and sequenced. Plasmids with the efficient gRNAs were delivered by electroporation to hESCs. Single cell CRISPR clone selection, expansion and sequencing protocols were adapted from Peters *et al* (Peters et al., 2008). Following FACS selection, GFP^+ hESCs were plated sparsely onto Matrigel coated dishes for growing single cell clones. After 10 days, individual clones were picked, plated into 96-well plates, and sequenced. Four clones harboring ASB2 gene locus modification along with four wild type (Wt) clones were expanded and differentiated into CMs for further analysis. 6 guides were tested individually (sequences below). Guides 1 and 6 were successful in inducing the knockouts.

Guides used were: Guide 1: 5' CACCGGTTGGTACATGCAGACGCGG 3' and 5' AAACCCGCGTCTGCATGTACCAACC 3'; Guide 2: 5' CACCGGTCCGCTAGGCTCTGCTCGA and 5' AAACTCGAGCAGAGCCTAGCGGACC 3'; Guide 3: 5' CACCGGGCCCCTTGTCTTGTCCGCT 3' and 5' AAACAGCGGACAAGACAAGGGGCCC 3'; Guide 4: 5' CACCGGCCCGGGCCGGCGAACTCTC 3' and 5' AAACGAGAGTTCGCCGGCCCGGGCC 3'; Guide 5: 5' CACCGCTCCTGAGAGTTCGCCGGCC 3' and 5' AAACGGCCGGCGAACTCTCAGGAGC 3'; Guide 6: 5' CACCGCTGCACGAGGCCGCATACTA 3' and 5' AAACTAGTATGCGGCCTCGTGCAGC 3'

Western blot analysis. Total protein extracts were prepared using RIPA buffer. Proteins were run on 10% TGX pre-cast gels from biorad and transferred to PVDF membranes using Trans-blot turbo transfer kit (Biorad). Membranes were blocked with 5% non-fat milk or BSA (in case of pSmad2) and primary antibodies were incubated overnight at 4^{o}C. Secondary antibodies linked to HRP (horseradish peroxidase) were incubated for 1 hour at room temperature and signal was revealed using super signal west femto or pico ECL substrates (Thermo-scientific). Antibodies used were Smad2 (5339, Cell Signaling), pSmad2 (3108, cell signaling) and Smad4 (ab40759, ABCAM). Western blots were then quantified using the Image Lab software.

Statistical Analysis: Standard t-test was used for the QPCR analysis and the heart tube measurements. One-way ANOVA was used for the western blot quantification as well as the percentages of Smad4 and pSmad2 positive cells where. $p<0.05$ is considered statistically significant.

Data and Software availability: RNAseq data have been deposited in NCBI's Gene Expression Omnibus (GEO) and can be accessed through GEO Series accession number GSE145495.

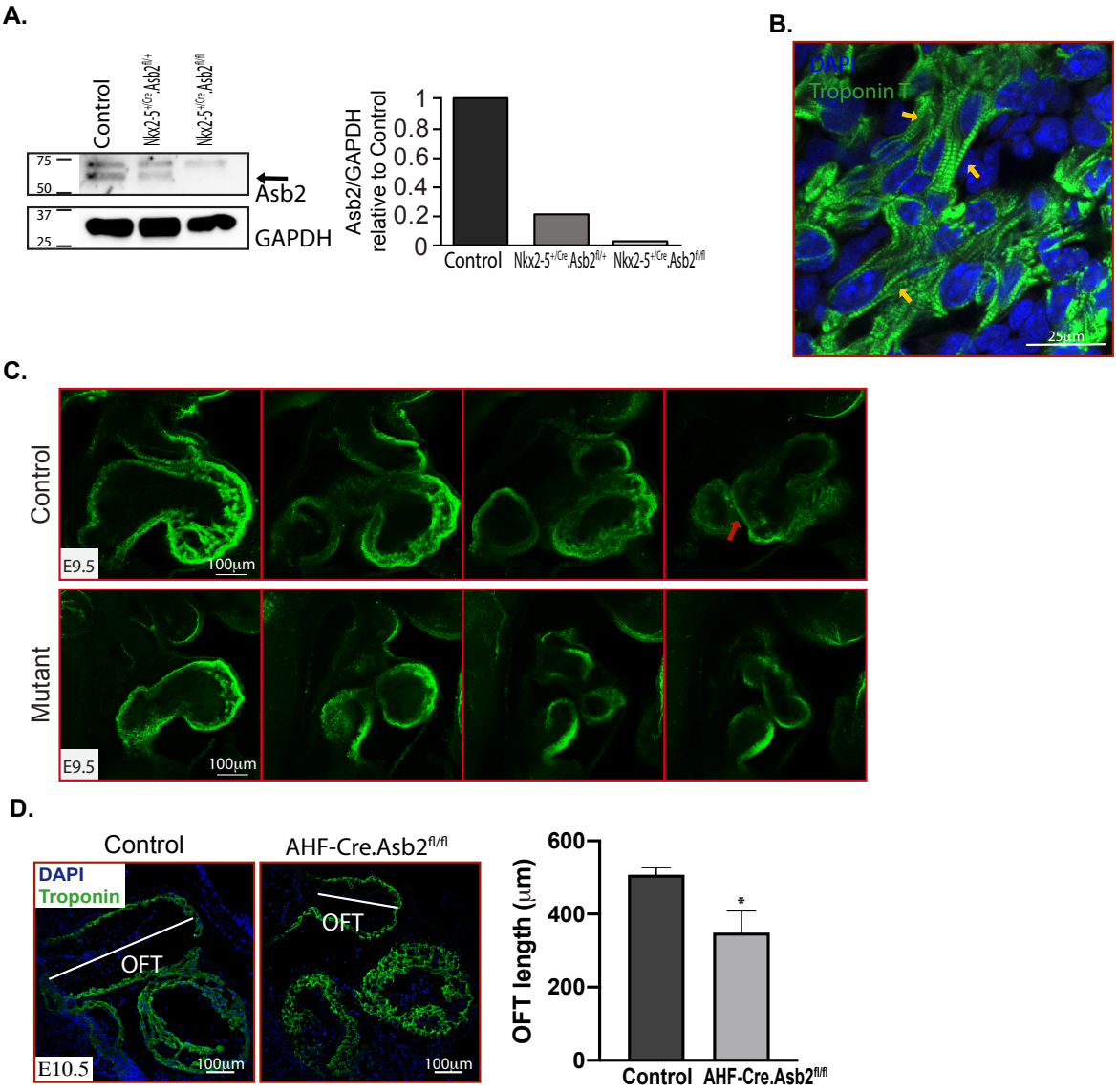

Supplementary figure 1, related to figure 2. A. Western Blot analysis on hearts of e9.5 Nkx2-5$^{+/Cre}$.Asb2$^{fl/+}$, Nkx2-5$^{+/Cre}$.Asb2$^{fl/fl}$, and their control littermates using Asb2 antibody and GAPDH for loading control. Notice reduced Asb2 protein levels in the heterozygous mice (fl/+) and the complete loss of Asb2 in the knockout mice (fl/fl) (quantification analysis on the rights) (5-6 hearts were uses per condition). **B & C.** CUBIC/Immunofluorescence of E9.5 mice embryos. **B.** High magnification showing the cardiac myocardial region of an E9.5 mouse embryo cleared with CUBIC and immuno-stained for Troponin T (green). Blue marls DAPI. Note the visible striations (yellow arrows). Scale bar is equivalent to 25µm. **C.** Serial sections of Control (top) and Mutant (bottom) E9.5 cleared/stained mice embryos, showing the heart region. Troponin T (green) was used to mark the myocardium. Note the bulging in the Control heart (right arrow) which is missing in the Mutant. **D.** Immunohistochemistry on E10.5 AHF-Cre.Asb2 hearts (AHF-Cre.Asb2$^{fl/fl}$, right panel) and littermate control (left panel) using Troponin-T (gree)-specific antibody. Note the shorter outflow tract (OFT) of the AHF-Cre.Asb2$^{fl/fl}$ heart. Scale bar is equivalent to 100µm. 4 Control and 3 knockout hearts were analyzed. *: p<0.005 significant vs. control. Unpaired t-test was used for analysis using Graphpad Prism.

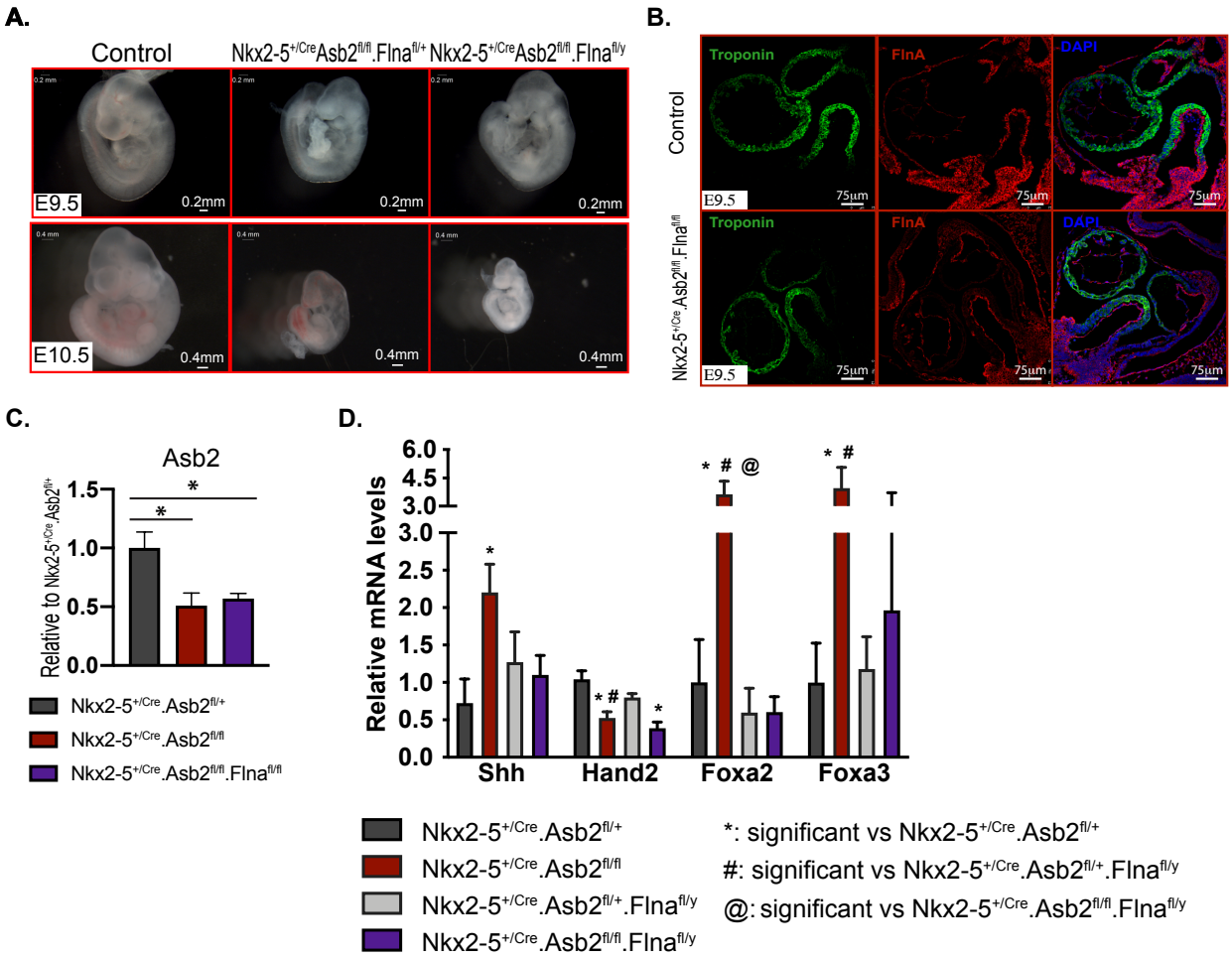

Supplementary Figure 2, related to figure 3. A. Nkx2-5+/Cre.Asb2.Flna E9.5 and E10.5 embryos. Note the smaller Nkx2-5$^{+/Cre}$.Asb2$^{fl/fl}$.Flna$^{fl/+}$ and Nkx2-5$^{+/Cre}$.Asb2$^{fl/fl}$.Flna$^{fl/y}$ at E9.5 and E10.5. Nkx2-5$^{+/Cre}$.Asb2$^{fl/fl}$.Flna$^{fl/+}$ and Nkx2-5$^{+/Cre}$.Asb2$^{fl/fl}$.Flna$^{fl/y}$ often presented with pericardial edema at both stages. 16 litters were analyzed at E9.5 and 3 litters at E10.5. Scale bar is equivalent to 0.2mm at E9.5 and 0.4mm at E10.5 embryos as indicated. **B.** Immunofluorescence on Nkx2-5$^{+/Cre}$.Asb2$^{fl/fl}$.Flna$^{fl/y}$ double knockouts and controls using Flna (red) and Troponin T (green) antibodies. Note absence of Flna expression in the myocardium of the double knockouts as opposed to its expression in the myocardium of the single knockouts in figure 3A. Scale bar is equivalent to 75µm. **C.** Asb2 transcipt levels from RNAseq data showing reduced Asb2 levels in the single and double knockouts compared to the Asb2 heterozygote control. *: $p<0.05$. One-way ANOVA was used for analysis using Graphpad Prism. **D.** QPCR analysis of hearts from Nkx2-5$^{+/Cre}$.Asb2$^{fl/+}$, Nkx2-5$^{+/Cre}$.Asb2$^{fl/fl}$, Nkx2-5$^{+/Cre}$.Asb2$^{fl/+}$.Flna$^{fl/y}$, Nkx2-5$^{+/Cre}$.Asb2$^{fl/fl}$.Flna$^{fl/y}$ E9.5 mice. N=5-6 for Nkx2-5$^{+/Cre}$.Asb2$^{fl/+}$; n=5 for Nkx2-5$^{+/Cre}$.Asb2$^{fl/fl}$; n=5-6 for Nkx2-5$^{+/Cre}$.Asb2$^{fl/+}$.Flna$^{fl/y}$; n=3 for Nkx2-5$^{+/Cre}$.Asb2$^{fl/fl}$.Flna$^{fl/y}$ (each sample is a combination of 2-3 hears to account for littermate variability). The selected genes are among those identified in RNAseq analysis in fugures 2 and 3. $P<0.05$ is considered statistically significant. T-test was used for analysis using Graphpad Prism.

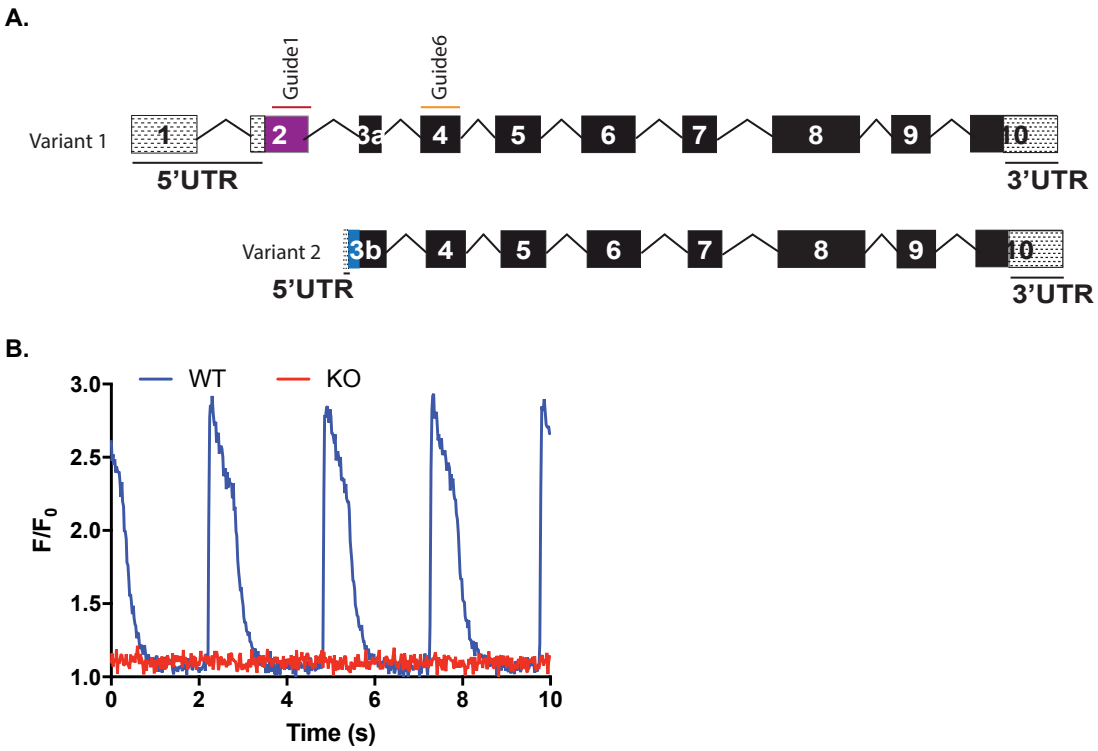

Supplementary Figure 3, related to figure 7. A. Schematic representation of the two Asb2 isoforms showing the location of the guides used for CRISPR/Cas9 genome editing. **B.** Representative calcium transients of hiPSC-CMs (WT: blue, KO: red).